PCCP

Accepted Manuscript

ROYAL SOCIETY OF CHEMISTRY

www.rsc.org/pccp

A Density Functional Theory Insight Towards Rational Design of Ionic Liquids for SO_2Capture

Gregorio García,[a] Mert Atilhan,[b] Santiago Aparicio*[a]

[a] Department of Chemistry, University of Burgos, 09001 Burgos, Spain

[b] Department of Chemical Engineering, Qatar University, P.O. Box 2713, Doha, Qatar

*Corresponding author: e-mail:sapar@ubu.es

ABSTRACT

A systematic Density Functional Theory (DFT) analysis has been carried out to obtain information at the molecular level on the key parameters related with efficient SO_2 capture by ionic liquids (ILs). A set of 55 ILs, for which high gas solubility are expected, has been selected. SO_2 solubility of ILs was firstly predicted based on COSMO-RS (Conductor-like Screening Model for Real Solvents) method, which provides a good prediction of gas solubility data in ILs without prior experimental knowledge of the compound's features. Then, interactions between SO_2 and ILs were deeply analyzed through DFT simulations. This work has shed valuable information about required factors at the molecular level to provide high SO_2 solubility in ILs, which is crucial for further implementation of these materials in the future. In our opinion, systematic researches on ILs for SO_2 capture allow increase our knowledge about those factors which could be controlled at the molecular level, allowing an approach up to the rational design of task-specific ILs.

1. INTRODUCTION

Air pollution is attracting an increasing attention throughout the world. Among the main air pollutants, sulfur dioxide (SO_2), which is mainly emitted through the combustion of fossil based fuels, is causing a serious harm to the environment and human health.[1, 2] At the same time, SO_2 is a useful source for many intermediates in chemical synthesis.[3] As matter of fact, there is a general interest in the design and improvement of methods for SO_2 capture. Although several methods have been developed for this purpose, all of them have several drawbacks. For instance, an effective method based on flue gas desulfurization (FGD) needs a large amount of water and subsequent treatment of the consequent waste, in order to prevent excessive amount of calcium sulphate that leading to a secondary pollution in the environment. Other methods, such as amine scrubbing, are affected by solvent loss and degradation due to the low volatility and stability of aminesolutions.[2, 4, 5]

In recent years, ionic liquids (ILs) have demonstrated their effectiveness for acid-gas removal from flue gas such as SO_2[2, 3, 5-9] and CO_2.[8-14] In addition, ILs contain unique properties, including good thermal and chemical stability, non-flammability and most distinctly they have almost null vapor pressure. All these features have been proved to be useful in chemical processes to replace volatile organic compounds. Nonetheless, the major advantage of ILs is the possibility to design task-specific solvents through the adequate cation-anion combinations, which requires a deep understanding on structure-property relationships.[9, 15] There is a large collection of compounds (approximately about ~10^6 when considering only "pure" ILs), and thus, system approaches on the ability of ILs for acid gas capture are useful in the selection of ILs for SO_2 storage. Unfortunately, the larger number of ILs hinders to carry out systematic experimental studies on huge number of ILs, due to the economical and temporal cost as well as limited experimental resources. Having mentioned the cost of experimental difficulties and cost hurdles associated with broad screening of ILs for acid-gas removal, Density Functional Theory (DFT) simulations have proven their ability to provide valuable indications and guide to the experimentalists. As matter of fact, DFT is a suitable tool for the analysis on the interactions between ILs and gas molecules at the nanoscopic level, which allow a deeper knowledge on structure-property relationships. Most of the reported DFT studies only consider CO_2.[7, 12, 13, 16, 17] Though, some researches leading with SO_2 capture have been reported.[7, 17]

There are few recent works that address utilization of ILs for gas capture at the molecular level, especially SO_2 capture. Damas *et al.* have shown a systematic study of acid- and sour-gas mitigation alternatives (SO_2, CO_2 and H_2S) by using ILs through DFT

simulations which mainly focuses on imidazolium cation based ILs[17]. In this presented work, we broadened the study that was conducted by Damas *et al.* by including other cations such as piridinium or cholinium cations in combination with anions such as bis(trifluorosulfonyl)imide, triflate, or tetrafluoroborate as shown in Table 1 and Figure 1.

In our opinion, the analysis of those ILs with high efficiency for SO_2 capture through DFT tools should be a good starting point to shed some light on the main molecular factors related with efficient SO_2 capture. Unfortunately, experimental researches dealing with SO_2 capture by ILs are still scarce and reduced to a small number of selected ionic liquid. A key parameter in the selection of ionic liquid for SO_2 capture is the gas solubility. It is well known that gas solubility in ILs can be predicted based on COSMO-RS (Conductor-like Screening Model for Real Solvents) method. [18] The COSMO-RS predicts thermodynamics properties of solvents on the basis of uni-molecular quantum chemical calculations for the individual molecules, which provides a good prediction of gas solubility data in ILs without prior experimental knowledge on the compound's properties.[14] Thus, COSMO-RS is able to carry out fast screening on a huge number of ionic liquid, reducing the number of candidates for experimental studies, which also reduces try-and-error attempts, economical and temporal cost. Consequently, COSMO-RS method was firstly used to carry out a quickly screening on a big matrix of ILs. Then, deeply study on those ILs, which are expected to provide high SO_2 solubility according to COSMO-RS method, from a molecular point of view was done using DFT tools. The combination of a first screening to select efficient ILs for SO_2 capture using COSMO-RS analysis along to DFT analysis on the most adequate ILs have allowed us to obtain information about structure *vs.* property relations that control SO_2 solubility in ILs, which is crucial for the rational design of task-specific ILs for SO_2 absorption.

2. THEORETICAL METHODOLOGY

2.1. COSMO-RS method. Four different approaches can be performed to describe ionic liquids according COSMO-RS method. According to Palomar *et al.*, these approximations are labelled as: $[C+A]_{GAS}$, $[C+A]_{COSMO}$, $[CA]_{GAS}$ and $[CA]_{COSMO}$.[14] The [C+A] model uses isolated ions to simulate ionic liquids systems, while ion-paired structures are used in [CA]. System optimizations can be carried out in gas-phase using quantum chemistry methods (GAS subscript), or the continuum solvation COSMO model (COSMO subscript). $[C+A]_{GAS}$ approach (*i.e.* independent ionic structures optimized in gas phase) predicts gas solubility data in slightly better agreement with the experiments. Palomar *et al.* also concluded that all COSMOS-RS approaches provide similar good capability to predict Henry's law constants

for ionic liquid. Nonetheless, $[C+A]_{GAS}$ model allows to perform analysis with a reduced computational time, since only optimized ion structures in gas phase are needed, which is especially useful for screening purposes.

The $[C+A]_{GAS}$ model was employed in this work, which is based on two main steps: (i) quantum chemical optimization for the molecular involved species and (ii) COSMO-RS statical calculations. Firstly, the isolated ions and SO_2 were optimized at B3LYP/6-311+G(d,p) level using Gaussian 09 (Revision D.01) package,[19] which was also instructed to provide the COSMO files. For these structures, COSMO files were calculated at the BVP86/TZVP/DGA1 theoretical level and used as input in the COSMOthermX program[18] to estimate Henry's laws constant. The COSMO-RS model parameterization used for all calculations was BP_TZVP_C21-0111.

In this work, Henry's law constants (K_H) for SO_2 were selected as a measure of absorbing capability. Hernry's constants are directly calculated by COSMOthermX code. The detail of theory of COSMO-RS can be found in the original works of Klamt *et al.*[18] Briefly, Henry's law constants can be defined as the ratio between the liquid phase concentration of SO_2 and its partial vapour pressure in the gas phase:

$$K_H = P_i/x_i = \gamma_i^{\infty} P_i^S \quad (1)$$

where P_i and x_i are the partial vapour pressure of a compound i (SO_2 in our study) in the gas phase and its molar fraction in the liquid. γ_i^{∞} is the activity coefficient of the compound at infinite dilution, and P_i^S is the saturated pure compound vapor pressure of the gas. Those parameters are directly provided by COSMOthermX code.

2.2. DFT simulations. Systems composed by one isolated molecule (*i.e.* isolated ions and SO_2) up to system composed by both ions and SO_2 were optimized. Optimized minima were checked trough their vibrational frequencies. For those simulations wherein two or more molecules are present, different starting points were employed in order to study different relative dispositions, focusing our attention on the disposition of minimal energy. All these calculations were carried out using B3LYP-D2 functional. B3LYP[20] has been selected since it has been proven to show appreciable performance over previously studied wide range of systems,[21], while dispersion corrections (D2) are adequate since we dealt with systems with dispersive interactions such as hydrogen bonds.[22] In addition, other works dealing with the performance of dispersion corrected functionals to study ionic liquid concluded that dispersion correction could significantly decreased mean absolute deviations for binding energies up to 10.0 KJ mol^{-1} or lower in comparison with MP2 method.[23] All atomic

elements, except iodine, were described with the standard Pople basis set 6-311+G(d,p). For iodine, a small core Stuttgart-Dresden-Bonn effective core potential was used (SDB-cc-pVTZ).[24] Interaction energies (*BE*) related with SO_2 capture were computed as the energy difference between the complex and the sum of the energy of each component. For example, *BE* for IL···SO_2 was calculated as:

$$BE = E_{IL\text{-}SO2} - (E_{cat} + E_{ani} + E_{SO2}) \quad (2)$$

Binding energies were also estimated by considering the IL as a whole (*BE'*), *i.e*., the binding energy due to the interaction between the IL and the gas molecule:

$$BE' = E_{IL\text{-}SO2} - (E_{IL} + E_{SO2}) \quad (3)$$

where $E_{IL\text{-}SO2}$, E_{cat}, E_{ani}, E_{IL} and E_{SO2} stand for the energies of IL···SO_2, cation, anion, IL and SO_2, respectively. For those systems composed by two or more molecules, computed energies were corrected according to counterpoise method to avoid basis set supper position error (BSSE).[25]

It has been shown that there is a specific charge transfer interaction between SO_2 and the ions.[26] There are different methods to calculate charge distributions, such as Mulliken method,[27] whose basis set dependence is well known.[28] ChelpG scheme[29] has demonstrated its suitability for ILs.[12, 30] Thus, atomic charges were also computed according to both ChelpG and Mulliken schemes. Intermolecular interactions where analyzed in the framework of Bader's theory (Atoms in Molecules, AIM).[31] In this context, intermolecular interactions are characterized through critical points (CP). Although four kind of critical points were obtained, we focused on bond critical points (BCP), which raises the criteria for considering the presence of intermolecular interactions.[31] AIM analysis were carried out with MultiWFN code.[32] All above-mentioned calculations were carried out with Gaussian 09 (Revision D.01) package.[19]

3. RESULTS AND DISCUSSION

3.1. COSMO-RS analysis: Selection of the optimal IL family. As said, the first step in our study was the selection of an optimal family of ILs whit high SO_2 solubility. The SO_2 absorption capacities were evaluated in terms of Henry's law constants (K_H) predicted according COSMO-RS method. COSMO-RS is a predictive method for thermodynamic equilibrium of fluids, which uses a statistical thermodynamic approach based on the results of uni-molecular quantum chemical calculations. The efficiency of COSMO-RS to predict the solubility behaviour of different solutes in ILs was evaluated by comparing both experimental and computed (according COSMO-RS method) Henry's constants.[14, 18, 33, 34] Although some

publications have reported that COSMO-RS systematically overestimates the Henry's constants, it provides a reasonable linear fit between calculated and experimental values.[14, 34]

In this work, COSMO-RS approach has been used to perform a fast screening on SO_2 solubility in ILs. Although several properties, such as σ-surfaces, screening charge density, and σ-profiles, histograms of screening charge can be computed with COSMO-RS, we have focused on Henry's law constants for SO_2 as a measure of absorbing capability. For this, K_H (at 303K) were estimated for a matrix of $\simeq$ 7600 ILs formed through the combination of cations based on imidazoluim, piperidinium, choline, ammonium cations paired with anions such as halogens, phosphates, tetrafluoroborate,dicyanamide or bis(trifluorosulfonyl)imide (see Table 1S). In addition to low Henry's law constants, only those ILs with adequate viscosity profile for industrial applications as suitable ILs for SO_2 capture were considered. Thus, a set of 55 ILs (see Table1 and Figure 1) was selected for a deeper DFT analysis. Table 1 and Figure 2 gather the computed Henry's law constants of selected ionic liquids. All selected ILs yield K_H within the range $2.5 \cdot 10^5$ Pascal and $6.5 \cdot 10^5$ Pascal at 303K. These values are smaller (which means higher solubility) than those reported by Gonzalez-Miquel et al. (of around $30 \cdot 10^5$ Pascal - $60 \cdot 10^5$ Pascal) for CO_2 absorption.[35] Then, high efficiency for SO_2 capture can be expected for selected ILs. Note that most of selected ILs are based on cations such as imidazoluim, pyridinium or piperazinium and anions such as $[BF_4]^-$, $[PF_6]^-$, $[NTf_2]^-$triflate or halides. Then, the combination of these anions would be adequate to design ILs for SO_2 capture with high efficiencies.

3.2. DFT analysis. As a first approximation, SO_2 capture at the molecule level could be related with the strength of the interactions between the ions and SO_2 molecule. In this work, interaction strength has been mainly analyzed based on binding energies (*BE*). Prior to analyze SO_2 capture by selected ILs, ion$\cdots SO_2$ and ionic pairs were also briefly assessed. Such information could be useful to rationalize the behavior of IL$\cdots SO_2$ systems.

3.2.1. Ion$\cdots SO_2$ systems. Figure 3 shows computed binding energies (|*BE*|) for anion$\cdots SO_2$ interactions. In general, selected cations provide similar |*BE*|, whose values lie between 31.70 kJ mol^{-1} ($[BMPyr]^+$) and 42.92 kJ mol^{-1} ($[CH]^+$), except $[EtNH_3]^+$ which yields the largest cation$\cdots SO_2$ values, (|*BE*|=58.60 kJ mol^{-1}). In concordance with Damas's work, the biding energy for imizadolium family decreases upon alkyl side chain elongation. In fact, from $[EMIM]^+$ to $[HMIM]^+$, *BE* varies only 1.83 KJ mol^{-1}. However, larger alkyl side chains such as $[OMIM]^+$ and $[HdMIM]^+$ lead to a slight increase in *BE* upon chain elongation.

Anion···SO_2 binding energies are, in general, larger than, with values varying between 41.91 kJ mol^{-1} ($[NTf_2]^-$) and 123.37 kJ mol^{-1} ($[H_2PO_4]^-$). Some ions can be classified according their chemical structure (such as those based on phosphate or sulfate anions). Thus, |*BE*| of those ones based on dialkyl phosphate slight decreases ($\simeq$ 4.00 KJ mol^{-1}) upon alkyl chain elongation. Alkyl chain absence in $[H_2PO_4]^-$ leads to |*BE*| values 29.12 KJ mol^{-1} greater than $[Et_2PO_4]^-$. Similar pattern are noted for sulfate-based ions, wherein the presence of ethyl chain leads to a diminution of 16.48 KJ mol^{-1}. As concerns as halides, |*BE*| = 52.18 KJ mol^{-1} (in average). In order to compare *BE* values with experimental data, IL 22 ([EMIM][NTf_2]) has been selected as its CO_2 capture performance has been demonstrated experimentally.[11] According with Eq. 2, CO_2 capture by IL 22 yields |*BE*|' = 36.58 KJ mol^{-1}. This energy could be considered as a low limit, from which higher |*BE*| would be adequate to provide high SO_2 affinities.

It has been proven that there is a charge transfer interaction between SO_2 and the anion motif of ILs. This charge transfer interaction is proportional to the anion basicity and plays an important role on gas adsorption capacity.[26] Figure 4 collects the charge transfers between the cation / anion and SO_2 molecule. For cation (anion)···SO_2 systems, the total charge over SO_2 molecule takes positive (negatives) values, which means that charge is transferred from the SO_2 up to the cation (from the anion up to the SO_2). Broadly, charge populations according Mulliken scheme are smaller than those one computed using ChelpG model. According with ChelpG (Mulliken) atomic charges, charge transfer between cations and SO_2 molecule is, in average, 0.05 (0.05) electrons. Thus, van der Waals interactions are one of the main contribution to the |*BE*| for cation-SO_2 systems, which is in concordance with lower |*BE*| values than anion-SO_2 systems. Now, the total charge over SO_2 molecule is 0.23 (0.21) electrons for anion-SO_2 systems. These higher values are in concordance with greater anion appetency to interact with SO_2 molecule due to a charge transfer interactions. Figure 5 shows the relationship between binding energies and charge transfer of anion···SO_2 systems (similar pattern has not been found for cation···SO_2 systems), which follows a linear behavior for most anions.

3.2.2. Ionic Liquids. Figure 6 gathers computed |*BE*| of the isolated ionic pair and the charge transfer (CT) between ions according ChelpG scheme. Most ILs yield |*BE*| between 318.99 KJ mol^{-1} (IL 21) and 492.70 KJ mol^{-1} (IL 20), while ILs 25, 29, 31, 33 and 35 provides the smallest values, around 173.09 KJ mol^{-1}. As known, the columbic attraction between opposite charges is the main force between both ions forming the ionic liquid. Even

though, other intermolecular forces can also be present. Both the charge transfer and *BE* follow similar patterns (Figure 6), *i.e.*, the columbic interaction between both positive and negative charges is one of the main contributions to the binding energy. ILs with the smallest |*BE*|, *i.e.* IL 25, 29, 31, 33 and 35, are those wherein high charge transfer does not provide high binding energies, which points out that other interactions (such as hydrogen bonds) also represent an important contribution (intermolecular interactions between ions are below described for some ILs). ILs based on halide anions (45-55) shown increasing CT with the halide electronegativity. Those effects are stronger from chloride to bromide halides. CTs and binding energies depend on both cation and anion nature as well. For instance, those ILs based on imidazol cations and $[NTF_2]^-$ anions (except ILs 25 and 29) yield similar |*BE*| ($\simeq$ 339.0 KJ mol^{-1}).

3.2.3. SO_2 capture by Ionic Liquids. Binding energies of IL$\cdots SO_2$ systems have used as a measurement of the interaction strength between selected ILs and SO_2 molecule. Figure 7 collects |*BE*| (according Eq. 2) of IL$\cdots SO_2$ systems, which has been decomposed as a sum of the ionic pair, cation$\cdots SO_2$ and anion$\cdots SO_2$ contributions. Thus, using the optimized IL$\cdots SO_2$ geometries, contributions from cation-anion, cation$\cdots SO_2$ and anion$\cdots SO_2$ have been also calculated. *BE* energies were also estimated taking into account the ILs as a whole (Eq. 2, |*BE'*|). All this quantities are also joined in Figure 7. The largest contribution to the binding energy comes from the interaction between both ions. For an easier comparison, this contribution has been also represented in Figure 6. For most ILs, SO_2 molecule only induces a scarce weakening on the interaction between ions (lower |*BE*|). However, ILs with the lowest |*BE*| in absence of SO_2 (ILs 25, 29, 31, 33 and 35, see Figure 6) are those wherein SO_2 molecule steers to a strengthening on the interaction between ions. This is due to the phenomena that the new arrangement between ions in of SO_2 improves the interaction between both ions and their interactions with the gas molecule, which is described in detail below.

As concerns as ion$\cdots SO_2$ contributions, cation$\cdots SO_2$ one is, in general, much lower than anion$\cdots SO_2$ contributions. Even if, the behavior of both ion$\cdots SO_2$ contributions and its relationship with |*BE*|' depends on the analyzed IL. For instance, anion$\cdots SO_2$ contributions present similar value than |*BE*'| for ILs 1-6 (based on tetrafluoroborate anion) and 45-55 (based on halides), *i.e.*, anion$\cdots SO_2$ interactions stand for the main contribution to the total binding energies of these IL-SO_2 systems. Hence, for those ILs based on $[BF_4]^-$ (1-6) and halides (45-55) anions, the SO_2 adsorption process is mainly governed by the anion. For ILs

based on triflate, thiocianathe or dicinamide (ILs 36-44), the sum of both ion···SO_2 contribution yields similar values of |*BE*'|. In consequence, the SO_2 capture using ILs 36-44 would be guided by both ions. Based on average values, binding energies of cation/anion-SO_2 systems (Figure 3) yield values $\simeq$ 37.09 KJ mol^{-1} / 72.37 KJ mol^{-1}. However, cation/anion···SO_2 contributions to the binding energy (Figure 7) are of around 13.94 KJ mol^{-1} / 52.03 KJ mol^{-1}. For both ions, interaction energies reduce $\simeq$ 21.9 KJ mol^{-1} due to the presence of the paired ion. Ions became less negative, since they transfer charge up to both the cation and SO_2 molecule. However, both ions strongly interact between them, hindering cation/anion···SO_2 interactions. Afresh, this general trend depends on the selected family. For example, for $[BF_4]^-$ / $[Cl]^-$ / $[Br]^-$ / $[I]^-$ anion |*BE*| = 55.45 KJ mol^{-1} / 54.64 KJ mol^{-1} / 50.07 KJ mol^{-1}/ 51.83 KJ mol^{-1}, while anion-SO_2 contributions to the total |*BE'*| for ILs 1-6 (which are those based on tetrafluoroborate anion) are $\simeq$ 69.28 KJ mol^{-1}, and $\simeq$ 90.07 KJ mol^{-1} for those ILs based on halides (45-55). As seen above, anion···SO_2 interactions are mainly ruled by the anion···SO_2. Both factors point out that the CT between both ions would increase anion basicity, as well as its interaction strength with the SO_2 molecule. Bearing in mind a value of around 36.0 KJ mol^{-1} (estimated for CO_2 capture by [EMIM][Tf_2N] IL) as a low limit, almost ILs yield larger values, |*BE'*| $\simeq$ 45.0 KJ mol^{-1}. According with these raised values, an efficient SO_2 capture can be expected. Once more, ILs 25, 29, 31, 33 and 35 do not follow the general trend, since their binding energies despising ionic contribution (|*BE*'|) are much larger than the sum of both ion···SO_2 contributions.

Total charges over both ions and SO_2 molecule are displayed in Figure 8. The gas usually gets a negative charge, *i.e.*, there is a charge transfer for the anion up to the SO_2 molecule. Charge populations over both ions for ILs in absence of SO_2 are also included in Figure 8. According with ChelpG scheme, cationic charges slight vary due to SO_2 molecule, while anionic charges suffer drastic lessening due to the charge transfer up to SO_2 molecule.

In short, anion···SO_2 interactions play an important role in SO_2 capture by ILs. When both ions are considered, anion···SO_2 strengths will be affected by cation-anion interactions. We have defined the binding energies of IL-SO_2 systems (*BE*, according Eq. 2) as a function of the *BE* of ion-SO_2 systems (section 3.2.1., Figure 3) and ionic pairs (section 3.2.2., Figure 6):

$$BE_{IL\text{-}SO2} = (aBE_{CAT\text{-}SO2})^x + (bBE_{ANISO2})^y + (cBE_{IL})^z \quad (4)$$

where $BE_{IL\text{-}SO2}$, $BE_{CAT\text{-}SO2}$, $BE_{ANI\text{-}SO2}$, BE_{IL} are the binding energies of the IL-SO_2, cation-SO_2, anion-SO_2 and anion-cation systems, while *a*, *b*, *c*, *x*, *y* and *z* are adjustable parameters. Figure 9a plots the results of a statistical analysis after expressing $BE_{IL\text{-}SO2}$ according with Eq. 4.

Figure 9a gathers the data collected for the whole set of ILs. Most of them yield a linear behavior between $BE_{IL\text{-}SO2}$ estimated from the IL-SO_2 optimized systems ($BE_{IL\text{-}SO2,DFT}$) and those one after the fit of Eq. 4 ($BE_{IL\text{-}SO2,Statistical}$). Hence, the total binding energy of IL-SO_2 systems, which takes into account both anion-cation and anion-SO_2 interactions, could be directly obtained through the optimization of ion···SO_2 systems and ILs. The fit yields R^2=0.6772 and medium deviation (MD) = 3.20 KJ mol^{-1}, which could be considered as acceptable value despite the variety in the chemical structure of selected ionic liquid. The largest errors correspond to ILs 25, 29, 31, 33 and 35 ($|BE_{IL\text{-}SO2,Statistical}| \simeq$ 360.0 KJ mol). As seen above, those ILs suffered and strengthening of the interaction between ions due to the presence of SO_2 molecule. According with Eq. 4, not important differences on binding energies for ILs are expected upon SO_2 presence. On the other hand, IL 20 ($|BE_{IL\text{-}SO2,Statistical}|$ = 578.34 KJ mol) is based on $[EtNH_3]^+$ cation. $[EtNH_3]^+$-SO_2 provided the highest binding energy among all studied cations. According with *a* parameter ($a = 1.28 \cdot 10^{-16}$), contribution from $BE_{CAT\text{-}SO2}$ is close to zero. Hence, above expression is only applicable for those ILs wherein the anion plays the main role on SO_2 capture and for those ILs which not suffers important geometrical arrangement in presence of the gas molecule. Note that *z* parameter is close to one. As a result, we defined Eq. 4 based only on $BE_{ANI\text{-}SO2}$ and $BE_{IL.}$ $BE_{IL\text{-}SO2,Statistical}$ as follows:

$$BE_{IL\text{-}SO2,statistical} = b(BE_{ANISO2})^y + cBE_{IL} \quad (5)$$

The fit was repeated despising ILs 20, 25, 29, 31, 33 and 35. As seen in Figure 9b, there is a notable improvement in the fit performance with R^2=0.7887 and MD = 2.55 KJ mol^{-1}. It could be concluded that SO_2 capture by ILs is mainly governed by ILs, while interactions between ions are also an important parameters. Since *BE* between ions is much higher than anion-SO_2 ones, BE_{IL} grants the most important contribution to $BE_{IL\text{-}SO2,statistical}$. Then, for those ILs with similar BE_{IL}, the efficiency in SO2 capture will be ruled by the anion. In addition, Eq. 5 allows estimating $BE_{IL\text{-}SO2}$ only through the optimization of anion-SO_2 and cation-anion systems, which can be considered a useful insight up the rational design of ILs for SO_2 capture.

3.2.4. Representative Ionic Liquids for SO_2 capture. Up to now, properties for IL···SO_2 interactions have been analyzed for the whole family of selected ILs based on binding energies. As seen, the SO_2 absorption capacity is often governed by anion···SO_2 interactions, although cations have also an important role. Even though, cation-SO_2 contributions to the total |*BE*'| are always lower than cation-SO_2 binding energies, while this general trend was not

found for anion···SO_2 contributions. For instance, anion··SO_2 contributions to the total |*BE'*| for ILs (1-4, which are based on imidazolium cations paired with tetrafluoroborate anion) are higher than binding energies for anion-$[BF_4]^-$ systems, while the opposite trend was noted for ILs 22-29 (also based on imidazol derived cations, but paired with $[NTf_2]^-$ anion). In addition, a statistical analysis has shown that *BE* of IL-SO_2 systems mainly depends on anion-SO_2 and cation-anion interactions. The diversity in the nature of both ions forming the family of studied ILs hinders the search of structure-property relationships. Therefore the IL family has been divided in six sets (labelled as I-VII, see Figures 2 and 7), wherein ILs within the same sets has similar features regarding the chemical structure of their ions. For each one, the most representative ILs have been selected, whose intermolecular interactions where analyzed within the context of AIM theory to obtain some information on SO_2 capture mechanism at the nanoscopic level.

Set I (ILs 1-13) includes ILs based on imidazolium ($[Im]^+$) or pyridinium ($[Py]^+$) cations paired with $[BF_4]^-$ or $[PF_6]^-$ anions. ILs based on imidazolium and $[BF_4]^-$ (ILs 1-4) yields similar $K_H \simeq 3.6 \cdot 10^5$ Pascal and $|BE'| \simeq 49.65$ KJ mol^{-1}. [Im][PF_6] based ILs (8-10) render something smaller K_H ($\simeq 2.7 \cdot 10^5$ Pascal); however this improvement in K_H is not observer on $|BE'|$ ($\simeq$ 45.19 KJ mol^{-1}). For pyridinium based ILs (5-7 and 11-13) The replacement of $[Im]^+$ by $[Py]^+$does not lead to important changes on K_H and $|BE'|$. Though, the alkyl chain length in the cation, as well as the presence of $[BF_4]^-$ or $[PF_6]^-$ anions have effect of thermophysical properties such as viscosity or density.[30, 36] ILs included in set I would provide similar SO_2 capture efficiency (based on K_H and $|BE'|$ values). As matter of fact, several papers highlight the effect on macroscopical properties as a function of the selected ions elsewhere.[30, 36, 37] In order to discuss the effects on different ions at the molecular level, besides of previously described parameters, the interaction mechanism of [BMIm][BF_4] (IL 2), [BMIm][PF_6] (IL 8), [B4MPy][BF_4] (IL 7) and [B4MPy][PF_6] (IL 13) have been deeply analyzed as representative compounds of this set. Intermolecular interactions were localized and featured trough AIM theory (we have focused on electronic density values, ρ, for the main intermolecular interactions). Figure 10 plots their optimized structures in presence of SO_2 molecule (optimized geometries for isolated ILs are not represented since the presence of SO_2 does not carry out important changes on the relative disposition between ions), whereas bond length and AIM features of intermolecular interactions are reported in Table 2. In absence of SO_2 molecule, several anion-cation interactions are established. The main interactions are formed between F and H in position 2 of imidazolium/pyridinium ring, whose d (intermolecular distance) and ρ are $\simeq$ 2.240 and 0.0140 a.u., respectively. In this sense, it is

well known that the main interaction in imidazilium based ILs is carried out through the H atom in position 2.[17] The presence of SO_2 molecule leads to an intermolecular distance elongation and electronic density decrease, in concordance with lower |*BE*| of ILs using their geometries in presence of SO_2. As seen below, this effect is also noted for almost ILs under study. Anion-SO_2 interactions are mainly characterized by a BCP between F and S, labeled as d_6, d_{15}, d_{24} and d_{33} for ILs 2, 7, 8 and 13, respectively, whose ρ are 0.0273 a.u., 0.0189 a.u., 0.0135 a.u., 0.0092. a.u., respectively. Similar patterns are noted for anion-SO_2 contribution to the total binging energies (Figure 7). Cation-SO_2 interactions take place through O (SO_2) and H (cation). These H are mainly located on the alkyl side chain. For ILs based on $[B3MPy]^+$ / $[B4MPy]^+$ based ILs (6/7 and 12/13), the presence of methyl chain in position 3/4 brings slight improvement on K_H and *BE* respect to $[BPy]^+$. This methyl group in position 3/4 allows an additional intermolecular interaction (e.g., d_{13} for IL 7) with SO_2, which is absent for $[BPy]^+$.

ILs based on phosphate, sulfate, acetate or nitrate anions are located in set II. Most of them are also based on $[EMIm]^+$ cation. Interaction energies of anion$\cdots SO_2$ systems (see Figure 3), $[Et_2PO_4]^-$ (99.24 KJ mol^{-1}), $[EtSO_4]^-$ (65.75 KJ mol^{-1}), $[Ac]^-$ (120.47 KJ mol^{-1}) and $[NO_3]^-$ (85.06 KJ mol^{-1}), are larger than those estimated for $[EMIm]^+$ (33.77 KJ mol^{-1}) and $[EtNH_3]^+$ (58.60 KJ mol^{-1}) cations. Analogous behaviour are noted for both ion$\cdots SO_2$ contribution to the binding energy, i.e., anion$\cdots SO_2$ > cation$\cdots SO_2$. Nevertheless, the sum of both contributions is higher than |*BE'*| (see Figure 7). In concordance with |*BE*| computed for cation/anion$\cdots SO_2$, anion$\cdots SO_2$ contribution to the total *BE* are larger. Within of this set we have focused on $[EMIm]Et_2PO_4]$ (14), $[EMIm][EtSO_4]$ (17) and [EMIm][Ac] (19) ILs. A detailed analysis of $[CH][H_2PO_4]$ at the molecular level and their application for SO_2 capture will be studied in a separate work in the future. The structures of $[EMIm][Et_2PO_4]$ (14), $[EMIm][EtSO_4]$ (17) and [EMIm][Ac] (19) in presence and absence of SO_2 are reported in Figure 11. $[EtNH_3][NO_3]$ (20) IL has been also selected to obtain some insight up to the behaviour of this IL. In absence of SO_2 molecule, the main interaction between imidazolim cation and the corresponding anion is carried out an hydrogen bond between O atom (anion) and H in position 2 of imidazolium ring (labelled as d_1, d_8 and d_{16} for ILs 14, 17 and 19 respectively). Again, the presence of SO_2 molecule brings a diminution of the interaction between both ions. As seen in Figure 7 for IL 17, contribution from anion$\cdots SO_2$ interaction to the |*BE*| is larger than cation$\cdots SO_2$ own, which agrees with larger ρ values for d_{12} regarding to the interaction between cation and SO_2, i.e., d_{13} and d_{14} (similar behaviour can be drawn for ILs 14 and IL19). SO_2 molecule interacts with the anion through an intermolecular bond

between the S and one oxygen atom located in the anion. $[EtNH_3][NO_3]$ (20) presents the highest charge transfer and $|BE|$ between ions in absence of SO_2 (see Figure 6). As seen in Figure 11, there is a proton transfer between ions. In fact, the distance between $[NO_3]^-$ and H (d_{23}) is 1.045 Å, while the distance between N and this H (d_{24}) is 1.595 Å. ChelpG charges have shown that such O has a atomic charge of -0.58 (larger than the -0.46 e^- over the other O), while the positive charge over this H is 0.39 (charge over remaining H linked to N is of around 0.26 e^-). This effect is not observed in presence of SO_2 molecule. The adsorption of SO_2 by IL 20 is carried out by a strong interaction between SO_2 and the anion (d_{25}), while there are dual interactions between SO_2 and the cation (d_{26} and d_{27}, being the latter the weakness). Once more, a larger electronic density for d_{35} (respect to d_{26}) agrees with the greater contribution from $SO_2\cdots$interaction to $|BE'|$.

ILs based on $[NTf_2]^-$ anion (set III) are the largest group, whose $K_H \simeq 3.4\cdot10^5$ Pascal and $|BE'| \simeq 38.45$ KJ mol^{-1} (despising ILs 25, 29, 31, 33 and 35). For ILs 25, 29, 31, 33 and 35, $|BE'|$ is much larger than sum of both ion$\cdots SO_2$ contributions. Furthermore, ILs 25, 29, 31, 33 and 35 are the only ones whose interactions between ions are strengthened in presence of SO_2 molecule (see Figure 6). The SO_2 brings a rearrangement between ions which improves their mutual interaction and also their interactions with SO_2. To obtain information about this fact, we have focused on ILs $[BMIm][NTf_2]$. Optimized geometries as well as main results from intermolecular interaction analysis are collected in Figure 12 and Table 4. $[BMIm][NTf_2]$ ILs yields five intermolecular interactions (d_1-d_5) between both ions, wherein those one between the N (anion) and the H (cation) is position 2 is the strongest one. Although the same interactions between both ions are found in presence of SO_2 molecule, all of them suffer an elongation/decrease on intermolecular distances / electronic density values. SO_2 molecule is able to for two bonds with the anion, *i.e.*, d_6 (S$\cdots$O) and d_7 (S$\cdots$F), being the latter much weaker than S$\cdots$O interaction. Further, two O$\cdots$H bonds (d_8 and d_9) are noted between SO_2 and cation molecules. Although SO_2 brings a weakening on the interaction between ions (based on electronic density values), it also allows the formation of a cage, with their corresponding cage critical points (CCP). Concretely, two cage critical points (represented as purple points along *yz* view) are found, whose electronic density are 0.0027a.u.and 0.0018 a.u. The presence of both CCP points out to a charge delocalization process between different motifs. Results described for this IL could be extrapolated to ILs 29, 31, 33 and 35, i.e., larger $|BE'|$ values and stronger interaction between ions are due to charge delocalization process. This charge delocalization brings an increase on inter ionic interaction (respect to isolated IL),

and |*BE*'| is high than the sum of both ion···SO_2 contributions. Although, CCPs are also found for other ILs, they own much lower electronic density values.

ILs based on triflate anion ($[SO_3CF_3]^-$) are within of set IV (IL 36-40). Those ones also based on imidazolium cations (36-39) provide $K_H \simeq 4.22 \cdot 10^5$ Pascal and $|BE'| \simeq 60.30$ KJ mol^{-1}, which is due to the sum of both ion···SO_2 contribution. [BMPyr][SO_3CF_3] (IL40) yields $K_H = 3.57 \cdot 10^5$ Pascal and $|BE'| = 51.97$ KJ mol^{-1}, mainly due to the anion···SO_2 contribution. Larger anion···SO_2 contributions (Figure 7) to the binding energy mimics the previously reported compound for ion···SO_2 binding energies (Figure 3). Figure 13 and Table 5 gather optimized geometries and intermolecular parameters for [BMIm][SO_3CF_3] (37). Results obtained for this IL could be extrapolated for the whole set IV. The main interaction between both ions takes places through O corresponding to the anion and H in position 2 located in the cation (d_1), whose ρ and distances are more affected by SO_2 molecule, which brings its weakening. However, the remaining interactions are slightly affected by gas molecule. Thus, binding energy for IL 37 is very similar than contribution from inter ionic interaction to the *BE* estimated for IL 37···SO_2 system (see Figure 6). The adsorption of SO_2 by IL 37 is mainly carried out through O (anion)···S(SO_2) interaction (labelled as d_5). Even if, SO_2 molecule also owns two intermolecular O···H bonds with alkyl H atoms located in the cation (d_6 and d_7). In concordance with ion···contributions to |*BE'*|, anion···SO_2 interaction (based on its larger electronic density value) is greater than cation···SO_2 ones.

Set V (IL 41 44) comprises those ILs whose anions have at least one C=N group, *i.e*, thiocianate ($[SCN]^-$) and dicyanamide ($[DCA]^-$). ILs based on imidazolium cation (41-43) supply $K_H \simeq 4.23 \cdot 10^5$ Pascal and $|BE'| \simeq 76.21$ KJ mol^{-1}, while [BMPyr][DCA] (IL 44) yields $K_H = 2.88 \cdot 10^5$ Pascal and $|BE'| = 68.20$ KJ mol^{-1}. Isolated ions provided $|BE| = 78.40$ KJ mol^{-1} and 61.29 KJ mol^{-1}, while |*BE*| for imidazolium and [BMPyr]+ are $\simeq 36.99$ KJ $mol^{-1}$and 31.70 KJ mol^{-1}, respectively. Anew, the trend perceived for the interaction between anions (cation) and SO_2 in absence of the cation (anion) is also found for both ion···SO_2 contributions to the binding energies. [EMIM][SCN] (41) brings a |*BE'*| similar than anion···SO_2 contribution, while |*BE'*| for $[DCA]^-$ based ILs comes from both ion···SO_2 contribution. Figure 14 and Table 6 reports optimized geometries for [EMIm][SCN] (41), [EMIm][DCA] (42) and [BMPyr][DCA] (44). As expected (in absence of SO_2), both ions interact with $[EMIM]^+$ cation through its H in position 2. S and N terminal atoms from $[SCN]^-$ anion are able to interact whit this H atoms (d_1 and d_2). Further, S atom also provides an intermolecular interaction with methyl hydrogen (d_3). Although, $[DCA]^-$ owns two CN groups, only one of them interacts with H in position 2 (d_8), even though two interactions with alkyl H atoms are

also found (d_9 and d_{10}). Regarding to IL 44, only one N group interacts with the main position provided by the cation (d_{14}), although other intermolecular H bonds (with lower ρ) are also present (d_{15}-d_{18}). According with electronic density values, ionic interactions are stronger for $[SCN]^-$ anion, which agrees with its higher $|BE|$ vales (see Figure 6). ILs 41, 42 and 44 show similarities regarding to the interactions with the gas molecule. Thus, the main interaction is carried out between one terminal N (anion) and the central S atom (d_5, d_{11} or d_{19} for IL 41, 42 or 44, respectively). Although electronic density for d_5 (0.387 a.u.) is smaller than electronic density for d_{11} and d_{19} ($\simeq$ 0.423 a.u.), larger charge transfer from the $[SCN]^-$ anion up to the gas (see Figure 8) agrees with greater $[SCN]^-\cdots SO_2$ contribution in IL41-SO_2 system (Figure 7). SO_2 molecule also interacts (through both hydrogen atoms) with the cation (d_6 and d_7, d_{12} and d_{13} or d_{20} and d_{21} for IL 41, 42 or 44, respectively. Instead the selected IL, the sum of the electronic density for both intermolecular bonds is $\simeq$ 0.0190 a.u. Thus, cation$\cdots SO_2$ contribution to the *BE* is similar for all IL within of set V.

Set VI is devoted to those ILs based on imidazolium cations and halides (IL 44-55). Keeping constant the halide, $[EMIM]^+$ cation always provides the lowest K_H values, while for the same cation K_H increases from chloride to bromide. Similar trends are noted for $|BE'|$ (see Figure 7), *i.e.*, high K_H is related with low $|BE'|$. The elected halides in this work gave $|BE|$ values ($\simeq$ 52.18 KJ mol^{-1}) lower than other anions; even though this $|BE|$ is larger than those one obtained for imidazolium cations ($\simeq$ 35.99 KJ mol^{-1}). For ILs 45-55, cation$\cdots SO_2$ and anion$\cdots SO_2$ contributions take values of around 8.00 KJ $mol^{-1}$and 88 KJ mol^{-1}. Halide effects on the SO_2 adsorption mechanism has been analyzed for ILs based on $[EMIM]^+$ cation as a function of the anion. Optimized structure for [EMIM][Cl]and [EMIM][Br] (optimized structures for [EMIM][[I] is not displayed since similar results to [EMIM][Br] are obtained) are shown in Figure 15, while main structural parameter of intermolecular interactions along their electronic density values are collected in Table 7. As expected, the main interaction between both ions is a hydrogen bond between the halide and the H atom located in position 2 (d_1 or d_6 for IL 45 or 48/51, respectively), which is weakened in presence of SO_2 molecule. For IL$\cdots SO_2$ systems, S$\cdots$X (X = Cl, Br or I) is the main interaction (labelled as d_3 or d_9 for IL 45 or 48/51, respectively), while two O$\cdots$H intermolecular bonds are also found between SO_2 and the cation. As seen in Table 6, electronic density for d_6 is much greater than those one of cation$\cdots SO_2$ interactions in concordance with its larger contribution from $[Cl]^-\cdots SO_2$ interaction. The same behaviour is also noted for ILs 48 and 51.

4. CONCLUSIONS

This contribution reports a Density Functional Theory (DFT) on several ILs, for which high SO_2 solubility is expected. This work is divided in three parts: *i*) we selected a set of ILs which should provided high efficiency for SO_2 capture. For this, a screening on a big number of ILs via COSMO-RS method was done; *ii*) Binding energies between SO_2 and ILs were analyzed intensely through DFT simulations for a set of 55 ILs, whose provided high efficiency in SO_2 capture according COSMO-RS method; *iii*) Intermolecular interaction for some representative ILs were deeply studied through AIM theory aimed at obtaining some information on the SO_2 adsorption mechanism at the molecular level. The results evidenced the ability of selected cations and anions to interact with SO_2 molecule, which is stronger for anion$\cdots SO_2$ interactions. Thus, anion$\cdots SO_2$ interactions are ruled by a strong charge transfer from the anion to SO_2 molecule. For the ILs$\cdots SO_2$ system, the total binding energy (*BE*) has been decomposed in the contributions from the interactions between ions, anion$\cdots SO_2$ and cation$\cdots SO_2$. The interaction between both ions always provided the largest contribution to the total binding energy. Then, the binding energy related with SO_2 capture by ILs was also calculated considering the ILs as a whole (*BE*'). A value of around 36.58 KJ mol^{-1} (for CO_2 capture by [EMIM][NTf_2] IL, which was taken as a pivotal reference for comparison purposes) as a low limit; all ILs yield larger binding energies. Most of them provide values of around 45.0 KJ $mol^{-1.}$ Therefore, all of them would provide high SO_2 capture efficiency. Through the comparison between ion$\cdots SO_2$ contributions and *BE*', we could obtain some information on what ion mainly govern the SO_2 capture within the ILs. In most cases, SO_2 capture at would be mainly ruled out by the anion or by both ions. Even if the SO_2 capture mechanism at the molecule level depends on each ILs, some common features as found for related ions. Even though, a statistical analysis of binding energies of IL-SO_2 systems as a function of ion-SO_2 and cation-anion ones brings to light that SO_2 adsorption by ILs at the molecular level is mainly ruled by anion-SO_2 interaction and cation-anion as well. Thus, qualitative trends on SO_2 capture by ILs can be obtained only based on the study of anion-SO_2 and isolated ILs systems. Systematic research on ILs for SO_2 capture allow increase our knowledge about those factors which could be controlled at the molecular level, allowing an approach up to the rational design of task-specific ILs for future applied studies.

ACKNOWLEDGMENTS

Gregorio García acknowledges the funding by Junta de Castilla y León (Spain), cofunded by European Social Fund, for a postdoctoral contract. Santiago Aparicio acknowledges the funding by Ministerio de Economía y Competitividad (Spain, project CTQ2013-40476-R)

and Junta de Castilla y León (Spain, project BU324U14). Mert Atilhan acknowledges support of an NPRP grant (No:6-330-2-140) from the Qatar National Research Fund. The statements made herein are solely the responsibility of the authors.

REFERENCES

1. S. J. Smith, J. van Aardenne, Z. Klimont, R. J. Andres, A. Volke, S. Delgado Arias, *Atmos. Chem. Phys.,* 2011, **11**, 1101-1116.
2. G. Cui, C. Wang, J. Zheng, Y. Guo, X. Luo, H. Li, *Chem. Comm.,* 2012**, 48**, 2633-2635.
3. J. Huang, A. Riisager, P. Wasserscheid, R. Fehrmann, *Chem. Comm.,* 2006 , 4027-4029.
4. Z. Z.Yang, L. N. He, Y. N. Zhao, B. Yu, *Environ. Sci. Technol.,*2013**, 47**, 1598-1605.
5. Yang, D.; Hou, M.; Ning, H.; Ma, J.; Kang, X.; Zhang, J.; Han, B., Reversible Capture of SO2 through Functionalized Ionic Liquids. *ChemSusChem* **2013,** *6* (7), 1191-1195.
6. S. Tian, Y. Hou, W. Wu, S. Ren, C. Zhang, *RSC Advances* 2013**, 3**, 3572-3577; X. L. Yuan, S. J. Zhang, X. M. Lu, *J. Chem. Eng. Data,* 2007**, 52**, 596-599; S. Ren, Y. Hou, W. Wu, Q. Liu, Y. Xiao, X. Chen, *J. Phys. Chem. B,* 2010**, 114**, 2175-2179; G. Cui, J. Zheng, X. Luo, W. Lin, F. Ding, H. Li, C. Wang,Angew. Chem. Int. Ed., 2013**, 52,** 10620-10624.
7. G. Yu, X. Chen, *J. Phys. Chem. B,* 2011**, 115**, 3466-3477.
8. S. Ren,Y. Hou, S. Tian, X. Chen, W. Wu, *J. Phys. Chem. B,* 2013**, 117,** 482-2486.
9. Z. Lei, C. Dai, B. Chen, *Chem. Rev.,* 2013**,** 114, 1289-1326.
10. S. Aparicio, M. Atilhan, *Energy & Fuels,* 2010**, 24**, 4989-5001; S. Aparicio, M. Atilhan, *J. Chem. Phys. B* **2012,** *116*, 9171-9185; F. Karadas, M. Atilhan, S. Aparicio, *Energy & Fuels,* 2010, **24**, 5817-5828; D. H. Zaitsau, A. V. Yermalayeu, S. P. Verevkin, J. E. Bara, A. D. Stanton, *Ind. Eng. Chem. Res.,* 2013**, 52**, 16615-16621; C. Wang, X. Luo, H. Luo, D. E. Jiang, H. Li, S. Dai, *Angew. Chem. Int. Ed.,* 2011**, 50**, 4918-4922; X. Zhang, H. Dong, Z. Zhao, S. Zhang, Y. Huang, Y., Carbon capture with ionic liquids: overview and progress. *Energy Environ. Sci.,* 2012**, 5**, 6668-6681.
11. F. Karadas, B. Köz, J. Jacquemin, E. Deniz, D. Rooney, J. Thompson, C. T. Yavuz, M. Khraisheh, S. Aparicio, M. Atilhan, *Fluid Phase Equilibria*, 2013**, 351**, 74-86.
12. V. Sanz, R. Alcalde, M. Atilhan, S. Aparicio, *Journal of Molecular Modeling,* 2014**, 20**, 1-14.
13. S. Aparicio, M. Atilhan, M. Khraisheh, R. Alcalde, J. Fernández, *J. Phys. Chem. B,* 2011**, 115**, 12487-12498.
14. J. Palomar, M. González-Miquel, A. Polo, F. Rodríguez, *Ind. Eng. Chem. Res.,* 2011**, 50**, 3452-3463.
15. J. Earle-Martyn, R. Seddon-Kenneth, Green Solvents for the Future. In *Clean Solvents*, American Chemical Society: 2002; J. S. Wilkes, *Green Chemistry*, 2002**, 4**, 73-80; R. D. Rogers, K. R. Seddon, *Science*, 2003**,** , 792-793.
16. O. Hollóczki, Z. Kelemen, L. Könczöl, D. Szieberth, L. Nyulászi, A. Stark, B. Kirchner, B. *ChemPhysChem*, 2013**, 14**, 315-320; K. M. Gupta, J. Jiang, *J. Phys. Chem. C,* 2014**, 118**, 3110-3118; P. Gu, R. Lü, S. Wang, Y. Lu, D. Liu, *Computational and Theoretical Chemistry,* 2013**, 1020**, 22-31; F. Yan, M. Lartey, K. Damodaran, E. Albenze, R. L. Thompson, J. Kim, M. Haranczyk, H. B. Nulwala, D. R. Luebke, B. Smit, *Phys. Chem. Chem. Phys.,* 2013**, 15**, 3264-3272; C. Wu, T. P. Senftle, W. F. Schneider, *Phys. Chem. Chem. Phys.,* 2012**, 14**, 13163-13170; B. Gurkan, B. F. Goodrich, E. M. Mindrup, L. E. Ficke, M. Massel, S. Seo, T. P. Senftle, H. Wu, M. F. Glaser, J. K. Shah, E. J. Maginn, J. F. Brennecke, W. F. Schneider, *J. Phys. Chem. Lett.,*2010**, 1**, 3494-3499.
17. G. B. Damas, A. B. A. Dias, L. T. Costa, *J. Phys. Chem. B,* 2014**, 118**, 9046-9064.
18. A. Klamt, *COSMO-RS: From Quantum Chemistry to Fluid Phase Thermodynamcis and Drug Design*. Elsevier: Amsterdam, 2005; F. Eckert, A. Klamt, *AIChE Journal* 2002**, 48**, 369-385.
19. M. J. Frisch, G. W. Trucks, H. B. Schlegel, G. E. Scuseria, M. A. Robb, J. R. Cheeseman, G. Scalmani, V. Barone, B. Mennucci, G. A. Petersson, H. Nakatsuji, M. Caricato, X. Li, H. P. Hratchian, A. F. Izmaylov, J. Bloino, G. Zheng, J. L. Sonnenberg, M. Hada, M. Ehara, K. Toyota, R. Fukuda, J. Hasegawa, M. Ishida, T. Nakajima, Y. Honda, O. Kitao, H. Nakai, T. Vreven, J. A. Montgomery, Jr., J. E. Peralta, F. Ogliaro, M. Bearpark, J. J. Heyd, E. Brothers, K. N. Kudin, V. N. Staroverov, R. Kobayashi, J. Normand, K. Raghavachari, A. Rendell, J. C. Burant, S. S. Iyengar, J. Tomasi, M. Cossi, N. Rega, J. M. Millam, M. Klene, J. E. Knox, J. B. Cross, V. Bakken, C. Adamo, J. Jaramillo, R. Gomperts, R. E. Stratmann, O. Yazyev, A. J. Austin, R. Cammi, C. Pomelli, J. W. Ochterski, R. L. Martin, K. Morokuma, V. G. Zakrzewski, G. A. Voth,

P. Salvador, J. J. Dannenberg, S. Dapprich, A. D. Daniels, Ö. Farkas, J. B. Foresman, J. V. Ortiz, J. Cioslowski, and D. J. Fox. Gaussian 09, Revision **D.01**, Gaussian, Inc.: Wallingford, CT, USA, 2009.
20. C. Lee, W. Yang, R. G. Parr, *Phys. Rev. B,* **1988,** *37*, 785-789;A. D. Becke, *J. Chem. Phys.,* 1993**, 98***, 5648*; A. D. Becke, *Phys. Rev. A,* 1988**, 38**, 3098-3100.
21. A. J. Cohen, P. Mori-Sánchez, W. Yang, *Chem. Rev.,* 2012**, 112**, 289-320.
22. S. Grimme, *J. Comput. Chem.,* 2006**, 27**, 1787-1799.
23. T. Schwabe, S. Grimme, *Phys. Chem. Chem. Phys.* **2007, 9**, 3397-3406; S. Zahn, B. Kirchner, *J. Phys. Chem. A.,* 2008**, 112**, 8430-8435; S. Grimme, W. Hujo, B. Kirchner, *Phys. Chem. Chem. Phys.,* 2012**, 14,** 4875-4883; E. I. Izgorodina, U. L. Bernard, D. R. MacFarlane, *J. Phys. Chem. A.,* 2009**, 113**, 7064-7072; S. Zahn, F. Uhlig, J. Thar, C. Spickermann, B. Kirchner, *Angew. Chem. Int. Ed.,* 2008**, 47**, 3639-3641.
24. J. Marten, W. Seichter, E. Weber, U. Bohme, *CrystEngComm,* 2008**, 10**, 541-547.
25. S. Simon, M. Duran, J. J. Dannenberg, *J. Chem. Phys.,* 1996**, 105**, 11024; S. F.Boys, F. Bernardi, *Molecular Physics,* 1970**,** 19, 553-566.
26. R. A.Ando, L. J. A. Siqueira, F. C. Bazito, R. M. Torresi, P. S. Santos, *J. Phys. Chem. B,* 2007**, 111,** 8717-8719; L. J. A. Siqueira, R. A. Ando, F. C. C. Bazito, R. M. Torresi, P. S. Santos, M. C. C. Ribeiro, *J. Phys. Chem. B,* 2008**, 112**, 6430-6435.
27. R. S. Mulliken, *J. Chem. Phys.* 1955**, 23**, 1833.
28. J. J. Philips, M. A. Hudspeth, Jr, P. M. Browne, J. E. Peralta, *Chem. Phys. Lett.,* 2010**, 495**, 146-150.
29. C. M. Breneman, K. B. Wiberg, *J. Comput. Chem.,* 1990**, 11**, 361-373.
30. I. Bandrés, R. Alcalde, C. Lafuente, M. Atilhan, S. Aparicio, *J. Phys. Chem. B,* 2011**, 115**, 12499-12513.
31. R. F. W.Bader, *Atoms in Molecules: a Quantum Theory*. Oxford, 1990.
32. T. Lu, F. Chen, *J. Comput. Chem.,* 2012**, 33**, 580-592.
33. J. Palomar, V. R. Ferro, J. S. Torrecilla, F. Rodríguez, *Ind. Eng. Chem. Res.,* 2007**, 46**, 6041-6048; J. Palomar, J. S. Torrecilla, V. R. Ferro, F. Rodríguez, *Ind. Eng. Chem. Res.,* 2009**, 48**, 2257-2265; A. Klamt, *Wiley Interdisciplinary Reviews: Computational Molecular Science,* 2011**, 1**, 699-709; M. A. Diedenhofen, A. Klamt, *Fluid Phase Equilibria,* 2010**, 294**, 31-38; X. Zhang, Z. Liu, W. Wang, *AIChE Journal,* 2008**, 54**, 2717-2728; M. B. Miller, D. L. Chen, H. B. Xie, D. R. Luebke, J. Karl Johnson, R. M. Enick, *Fluid Phase Equilibria,* 2009**, 287**, 26-32; R- Franke, B. Hannebauer, S. A. Jung, *Chemical Engineering & Technology,* 2010**, 33**, 251-257; N. A. Manan, C. Hardacre, J. Jacquemin, D. W. Rooney, T. G. Youngs, *J. Chem. Eng. Data,* 2009**, 54**, 2005-2022.
34. M. González-Miquel, J. Palomar, S. Omar, *Ind. Eng. Chem. Res.,* 2011**,** *50*, 5739-5748.
35. M. González-Miquel, J. Bedia, J. Palomar, F. Rodríguez, *J. Chem. Eng. Data,* 2014**, 59**, 212-217.
36. M. Atilhan, J. Jacquemin, D. Rooney, M. Khraisheh, S. Aparicio, *Ind. Eng. Chem. Res.,* 2013**, 52**, 16774-16785.
37. G. García, M. Atilhan, S. Aparicio, *Chem. Phys. Lett.,* 2014**, 610**, 267-272.

Table 1. Selected family of ionic liquids studied in this work along their estimated Henry's Law constants of SO_2 (K_H) at 303K predicted using COSMO-RS method.

Nº	Cation	Anion	Labelling	$K_H \cdot 10^{-5}$/ Pascal
1	1-Ethyl-3-methylimidazolium	Tetrafluoroborate	[EMIm][BF_4]	3.69
2	1-butyl-3-methylimidazolium	Tetrafluoroborate	[BMIm][BF_4]	3.55
3	1-hexyl-3-methylimidazolium	Tetrafluoroborate	[HMIm][BF_4]	3.47
4	1-Methyl-3-octylimidazolium	Tetrafluoroborate	[OMIm][BF_4]	3.35
5	1-Butylpyridinium	Tetrafluoroborate	[BPy][BF_4]	3.72
6	1-Butyl-3-methylpyridinium	Tetrafluoroborate	[B3MPy][BF_4]	2.96
7	1-Butyl-4-methylpyridinium	Tetrafluoroborate	[B4MPy][BF_4]	2.96
8	1-butyl-3-methylimidazolium	Hexafluorophosphate	[BMIm][PF_6]	2.76
9	1-hexyl-3-methylimidazolium	Hexafluorophosphate	[HMIm][PF_6]	2.65
10	1-Methyl-3-octylimidazolium	Hexafluorophosphate	[OMIm][PF_6]	2.61
11	1-Butylpyridinium	Hexafluorophosphate	[BPy] [PF_6]	2.79
12	1-Butyl-3-methylpyridinium	Hexafluorophosphate	[B3MPy][PF_6]	2.47
13	1-Butyl-4-methylpyridinium	Hexafluorophosphate	[B4MPy][PF_6]	2.46
14	1-Ethyl-3-methylimidazolium	Diethylphosphate	[EMIm][Et_2PO_4]	4.73
15	1,3-Dimethylimidazolium	Dimethylphosphate	[DMIm][Me_2PO_4]	4.07
16	Choline	Dihydrogenphosphate	[CH][H_2PO_4]	6.29
17	1-Ethyl-3-methylimidazolium	Ethylsulfate	[EMIm][$EtSO_4$]	4.63
18	1-Ethyl-3-methylimidazolium	Hidrogensulfate	[EMIm][HSO_4]	6.45
19	1-Ethyl-3-methylimidazolium	Acetate	[EMIm][Ac]	3.85
20	Ethylammonium	Nitrate	[$EtNH_3$][NO_3]	6.37
21	Triethylsulfonium	Bis[(trifluoromethyl)sulfonyl]imide	[Et_3S][NTf_2]	3.52
22	1-Ethyl-3-methylimidazolium	Bis[(trifluoromethyl)sulfonyl]imide	[EMIm][NTf_2]	3.63
23	1-methyl-3-propylimidazolium	Bis[(trifluoromethyl)sulfonyl]imide	[MPIm][NTf_2]	3.54
24	1,2-Dimethyl-3-propylimidazolium	Bis[(trifluoromethyl)sulfonyl]imide	[DMPIm][NTf_2]	3.19
25	1-butyl-3-methylimidazolium	Bis[(trifluoromethyl)sulfonyl]imide	[BMIm][NTf_2]	3.50
26	1-Butyl-2,3-dimethylimidazolium	Bis[(trifluoromethyl)sulfonyl]imide	[BDMIm][NTf_2]	3.18
27	1-hexyl-3-methylimidazolium	Bis[(trifluoromethyl)sulfonyl]imide	[HMIm][NTf_2]	3.50
28	1-Hexadecyl-3-methylimidazolium	Bis[(trifluoromethyl)sulfonyl]imide	[HdMIm][NTf_2]	3.69
29	1-Allyl-3-methylimidazolium	Bis[(trifluoromethyl)sulfonyl]imide	[AMIm][NTf_2]	3.56
30	1-Methyl-1-propylpyrrolidinium	Bis[(trifluoromethyl)sulfonyl]imide	[MPPyr][NTf_2]	3.39
31	1-Butyl-1-methylpyrrolidinium	Bis[(trifluoromethyl)sulfonyl]imide	[BMPyr][NTf_2]	3.36
32	1-Methyl-1-propylpiperidinium	Bis[(trifluoromethyl)sulfonyl]imide	[MPPipe][NTf_2]	3.33
33	1-Butylpyridinium	Bis[(trifluoromethyl)sulfonyl]imide	[BPy][NTf_2]	3.49
34	1-Butyl-3-methylpyridinium	Bis[(trifluoromethyl)sulfonyl]imide	[B3MPy][NTf_2]	3.29
35	1-Butyl-4-methylpyridinium	Bis[(trifluoromethyl)sulfonyl]imide	[B4MPy][NTf_2]	3.29
36	1-Ethyl-3-methylimidazolium	Triflate	[EMIM][SO_3CF_3]	4.41
37	1-butyl-3-methylimidazolium	Triflate	[BMIM][SO_3CF_3]	4.20
38	1-hexyl-3-methylimidazolium	Triflate	[HMIM][SO_3CF_3]	4.17
39	1-Methyl-3-octhylimidazolium	Triflate	[OMIM][SO_3CF_3]	4.11
40	1-Butyl-1-methylpyrrolidinium	Triflate	[BMPyr][SO_3CF_3]	3.57
41	1-Ethyl-3-methylimidazolium	Thiocianate	[EMIM][SCN]	4.17
42	1-Ethyl-3-methylimidazolium	Dicyanamide	[EMIM][DCA]	4.30
43	1-butyl-3-methylimidazolium	Dicyanamide	[BMIM][DCA]	4.22
44	1-Butyl-1-methylpyrrolidinium	Dicyanamide	[BMPyr][DCA]	2.88
45	1-Ethyl-3-methylimidazolium	Chloride	[EMIM][Cl]	2.01
46	1-butyl-3-methylimidazolium	Chloride	[BMIM][Cl]	3.42
47	1-Allyl-3-methylimidazolium	Chloride	[AMIM][Cl]	2.87
48	1-Ethyl-3-methylimidazolium	Bromide	[EMIM][Br]	2.24
49	1-butyl-3-methylimidazolium	Bromide	[BMIM][Br]	3.53
50	1,3-Dimethylimidazolium	Iodide	[DMIm][I]	3.39
51	1-Ethyl-3-methylimidazolium	Iodide	[EMIm][I]	3.03
52	1-methyl-3-propylimidazolium	Iodide	[MPIm][I]	3.70
53	1-butyl-3-methylimidazolium	Iodide	[BMIm][I]	4.07
54	1-hexyl-3-methylimidazolium	Iodide	[HMIm][I]	4.50
55	1-Allyl-3-methylimidazolium	Iodide	[AMIm][I]	4.07

Table2. Intermolecular distances (d) along their electronic density values (ρ) of [BMIm][BF_4] (2), [B4MPy][BF_4] (7), [BMIm][PF_6] (8) and [B4MPy][PF_6] (13) ionic liquids. See Figure 10 for labeling.

	IL		$IL\cdots SO_2$	
	d / Å	ρ / a.u.	d / Å	ρ / a.u.
2 - [BMIm][BF_4]				
d_1	2.233	0.0143	2.788	0.0076
d_2	2.106	0.0178	2.457	0.0121
d_3	2.502	0.0082	2.502	0.0091
d_4	2.873	0.0101	2.892	0.0102
d_5	2.222	0.0130	2.447	0.0100
d_6			2.531	0.0273
d_7			2.518	0.0087
d_8			2.118	0.0170
7 - [B4MPy][BF_4]				
d_9[a]	2.298	0.0129	2.910	0.0097
d_{10}	2.119	0.0173	2.549	0.0148
d_{11}[a]	2.671	0.0117	2.484	0.0081
d_{12}	2.322	0.0097	2.870	0.0105
d_{13}			2.479	0.0077
d_{14}	2.289	0.0120	2.706	0.0188
d_{15}			2.716	0.0089
d_{16}			2.496	0.0082
d_{17}			2.429	0.0097
8 - [BMIm][PF_6]				
d_{18}	2.406	0.0113	2.421	0.0116
d_{19}	2.320	0.0138	2.607	0.0101
d_{20}	2.413	0.0107	2.701	0.0067
d_{21}	2.479	0.0100	2.315	0.0118
d_{22}[b]	2.698	0.0142	2.803	0.0094
d_{23}	2.488	0.0097	2.648	0.0206
d_{24}			2.652	0.0135
d_{25}			2.209	0.0084
d_{26}			2.535	0.0071
d_{27}			2.548	0.073
13 - [B4MPy][PF_6]				
d_{28}	2.328	0.0116	2.363	0.0128
d_{29}	2.124	0.0167	2.078	0.0181
d_{30}	2.313	0.0113	2.481	0.0145
d_{31}[a]	2.588	0.0114	2.446	0.0095
d_{32}			2.698	0.0057
d_{33}			2.648	0.0092
d_{34}			2.955	0.0065
d_{35}			3.218	0.0059
d_{36}			2.718	0.0058

[a] For isolated IL, this interaction take places between F and H in position 2. [b] For isolated IL, this interaction takes places between F and C in position 2.

Table 3. Intermolecular distances (d) along their electronic density values (ρ) of [EMIm]Et_2PO_4] (14), [EMIm][$EtSO_4$] (17), [EMIm][Ac] (19) and [$EtNH_3$][NO_3] (20). See Figure 11 for labeling.

	IL		IL···SO_2	
	d / Å	ρ / a.u.	d / Å	ρ / a.u.
14 - [EMIm][Et_2PO_4]				
d_1	1.756	0.0299	1.793	0.0369
d_2	2.304	0.0120	2.780	0.0194
d_3	1.962	0.0253	2.119	0.0064
d_4			2.238	0.0575
d_5			2.510	0.0088
d_6			2.578	0.0087
d_7			2.242	0.0144
17 - [EMIm][$EtSO_4$]				
d_8	2.055	0.0231	2.052	0.0225
d_9	2.510	0.0095	2.500	0.0096
d_{10}	2.417	0.0103	2.513	0.0087
d_{11}	2.184	0.0159	2.555	0.0082
d_{12}			2.243	0.0396
d_{13}			2.419	0.0109
d_{14}			2.444	0.0081
d_{15}			2.576	0.0059
19 - [EMIm][Ac]				
d_{16}	1.654	0.0278	2.110	0.0205
d_{17}	2.352	0.0109	2.491	0.0097
d_{18}	2.002	0.0240	2.427	0.0104
d_{19}			2.189	0.0658
d_{20}			2.667	0.0077
d_{21}			3.665	0.0128
d_{22}			2.583	0.0082
20 - [EMIm][NO_3]				
d_{23}	1.596	0.0072	1.639	0.0564
d_{24}	1.045		2.625	0.0078
d_{25}			2.350	0.0454
d_{26}			1.820	0.0328
d_{27}			2.620	0.0074

Table 4. Intermolecular distances (d) along their electronic density values (ρ) of [BMIm][NTf_2] (25).See Figure 12 for labeling.

	IL		IL···SO_2	
	d / Å	ρ / a.u.	d / Å	ρ / a.u.
	25 - [BMIm][NTf_2]			
d_1	1.952	0.0303	2.020	0.0266
d_2	2.186	0.0150	2.419	0.0104
d_3	2.290	0.0130	2.352	0.0115
d_4	2.564	0.0063	2.594	0.0058
d_5	2.553	0.0024	2.623	0.0058
d_6			2.683	0.0218
d_7			3.208	0.0062
d_8			2.739	0.0068
d_9			2.479	0.0099

Table 5. Intermolecular distances (d) along their electronic density values (ρ) of [BMIm][SO_3CF_3] (37). See Figure 13 for labeling.

	IL		IL···SO_2	
	d / Å	ρ / a.u.	d / Å	ρ / a.u.
	37 -[BMIm][SO_3CF_3]			
d_1	2.025	0.0239	2.184	0.0070
d_2	2.280	0.0130	2.626	0.0109
d_3	2.520	0.0081	2.439	0.0089
d_4	2.594	0.0088	2.544	0.0351
d_5			2.476	0.0096
d_6			2.464	0.0107
d_7			2.451	0.0070

Table 6. Intermolecular distances (d) along their electronic density values (ρ) of [EMIm][SCN] (41),[EMIm][DCA] (42)and [BMPyr][DCA] (44). See Figure 14 for labeling.

	IL		IL···SO_2	
	d / Å	ρ / a.u.	d / Å	ρ / a.u.
41 -[EMIm][SCN]				
d_1	2.567	0.0152	2.572	0.0141
d_2	2.907	0.0142		
d_3	2.841	0.0092		
d_4	2.532	0.0093		
d_5			2.369	0.0387
d_6			2.506	0.0089
d_7			2.513	0.0107
42 -[EMIm][DCA]				
d_8	2.348	0.0137	2.480	0.0115
d_9	2.180	0.0177	2.395	0.0051
d_{10}	2.161	0.0181	2.535	0.0048
d_{11}			2.431	0.0430
d_{12}			2.376	0.0118
d_{13}			2.630	0.0074
44 - [BMPyr][DCA]				
d_{14}	2.750	0.0084	2.745	0.0088
d_{15}	2.462	0.0106	2.406	0.0097
d_{16}	2.689	0.0075	2.534	0.0117
d_{17}	2.550	0.0104	2.585	0.0103
d_{18}	2.294	0.0143	2.463	0.0105
d_{19}			2.464	0.0105
d_{20}			2.617	0.0103
d_{21}			2.448	0.0088

Table 7. Intermolecular distances (d) along their electronic density values (ρ) of [EMIm][Cl] (45),[EMIm][Br] (48)and [EMIM][I] (51). See Figure 15 for labeling.

	IL		IL···SO_2	
	d / Å	ρ / a.u.	d / Å	ρ / a.u.
45 - [EMIm][Cl]				
d_1	1.982	0.0264	2.515	0.0149
d_2	2.750	0.0096	2.681	0.0111
d_3			2.589	0.0474
d_4			2.668	0.0110
d_5			2.367	0.0115
48 - [EMIm][Br]				
d_6	2.798	0.0242	2.581	0.0157
d_7	2.865	0.0101		
d_8	2.861	0.0095	2.754	0.0117
d_9			2.709	0.0455
d_{10}			2.112	0.0189
d_{11}			2.321	0.0125
51 - [EMIm][I]				
d_6	2.987	0.0218	2.753	0.0149
d_7	3.041	0.0088		
d_8	3.075	0.0099	2.963	0.0095
d_9			2.775	0.0455
d_{10}			2.121	0.0182
d_{11}			2.383	0.0134

Figure Captions.

Figure 1. Chemical structure for the ions involved in the selected family of ionic liquids.

Figure 2. Inverse of Henry's Law constants of SO_2 in ILs ($1/K_H$) at 303K predicted using COSMO-RS method.

Figure 3. Computed Binding Energies (in absolute value, $|BE|$) of cation$\cdots SO_2$ (up) and anion$\cdots SO_2$ (bottom) systems.

Figure 4. Charge transfer of cation$\cdots SO_2$ (up) and anion$\cdots SO_2$ (bottom) systems.

Figure 5. Binding energies ($|BE|$) *vs* Charge transfer of anion$\cdots SO_2$ systems.

Figure 6. Computed binding energies (in absolute value, $|BE|$) of Ionic Pairs (black line), along charge transfer computed according ChelpG scheme (blue bar). Binding energies of ionic pairs using their geometries in presence of SO_2 are also collected (green line),

Figure 7. Computed binding energies (in absolute value, $|BE|$) of ILs$\cdots SO_2$ (orange line), along anion$\cdots SO_2$ contributions (red bar), cation$\cdots SO_2$ (blue bar) and cation$\cdots$anion (green bar). Computed binding energies of ILs$\cdots SO_2$ considering the IL as a whole are also collected (black line).

Figure 8. Computed charge over SO_2 (blue), cation (green) and anion (red) according ChelpG scheme. Dotted lines correspond to ion charge for isolated ILs.

Figure 8. Results from the fit of $BE_{IL\text{-}SO2}$ according to equations 4 and 5. |

Figure 10. Optimized geometries of [BMIm][BF_4] (2), [B4MPy][BF_4] (7), [BMIm][PF_6] (8) and [B4MPy][PF_6] (13) in presence of SO_2 molecule. Main intermolecular interactions are also displayed. Atom colour code: C (gray), oxygen (red) sulphur (yellow), hydrogen (white), nitrogen (blue), boron (pink), phosphorous (orange) and fluorine (light blue) . See Table 2 for a more detailed description on intermolecular interactions.

Figure 11. Optimized geometries of [EMIm]Et_2PO_4] (14), [EMIm][$EtSO_4$] (17), [EMIm][Ac] (19) and [$EtNH_3$][NO_3] (20). Main intermolecular interactions are also displayed. Atom colour code: C (gray), oxygen (red) sulphur (yellow), hydrogen (white), nitrogen (blue)and phosphorous (orange). See Table 3 for a more detailed description on intermolecular interactions.

Figure 12. Optimized geometries of [BMIm][NTf_2] (25), [BMPyr][NTf_2] (31) and [B4MPy][NTf_2] (35). Main intermolecular interactions are also displayed. Atom colour code: C (gray), oxygen (red) sulphur (yellow), hydrogen (white), nitrogen (blue) and phosphorous (orange). See Table 4 for a more detailed description on intermolecular interactions.

Figure 13. Optimized geometries of [BMIm][SO_3CF_3] (37) in presence of SO_2 (similar results are obtained for isolated IL). Main intermolecular interactions are also displayed. Atom colour code: C (gray), oxygen (red) sulphur (yellow), hydrogen (white), nitrogen (blue) and fluorine (light blue). See Table 5 for a more detailed description on intermolecular interactions.

Figure 14. Optimized geometries of [EMIM][SCN] (41), [EMIM][DCA] (42) and [BMPyr][DCA] (44). Main intermolecular interactions are also displayed. Atom colour code: C (gray), oxygen (red) sulphur (yellow), hydrogen (white), nitrogen (blue) and fluorine (light blue). See Table 6 for a more detailed description on intermolecular interactions.

Figure 15. Optimized geometries of [EMIm][Cl] (45) and [EMIM][Br] (48). Similar geometries are obtained for [EMIM][I] (51).Main intermolecular interactions are also displayed. Atom colour code: C (gray), oxygen (red) sulphur (yellow), hydrogen (white), nitrogen (blue), chloride (green) and bromide (garnet). See Table 7 for a more detailed description on intermolecular interactions.

Cations

1-Ethyl-3-methylimidazolium $[EMIm]^+$

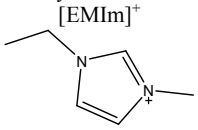

1,3-Dimethylimidazolium $[DMIm]^+$

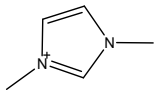

1-hexyl-3-methylimidazolium $[HMIM]^+$

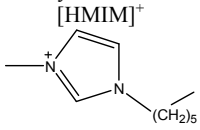

1-Methyl-3-octylimidazolium $[OMIm]^+$

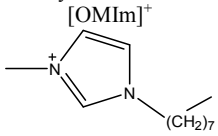

1-butyl-3-methylimidazolium $[BMIm]^+$

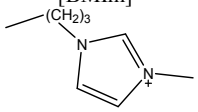

1-methyl-3-propylimidazolium $[MPIm]^+$

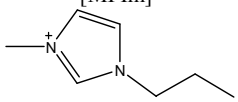

1-Hexadecyl-3-methylimidazolium $[HdMIm]^+$

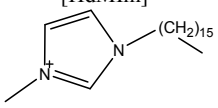

1-Allyl-3-methylimidazolium $[AMIm]^+$

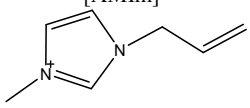

1-Butyl-2,3-dimethylimidazolium $[BDMIm]^+$

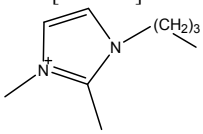

1,2-Dimethyl-3-propylimidazolium $[DMPIm]^+$

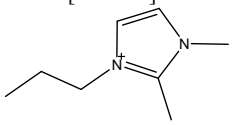

1-Methyl-1-propylpyrrolidinium $[MPPyr]^+$

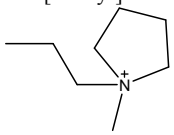

1-Butyl-1-methylpyrrolidinium $[BMPyr]^+$

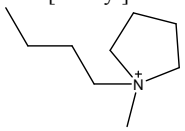

1-Butylpyridinium $[BPy]^+$

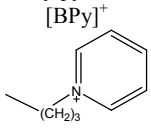

1-Butyl-3-methylpyridinium $[B3MPy]^+$

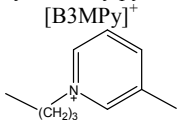

1-Butyl-4-methylpyridinium. $[B4MPy]^+$

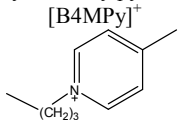

1-Methyl-1-propylpiperidinium $[MPPipe]_+$

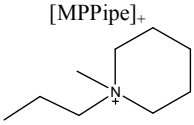

Choline $[CH]^+$

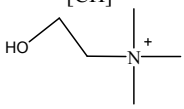

Ethylammonium $[EtNH_3]^+$

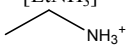

Triethylsulfonium $[Et_3S]^+$

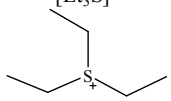

Anions

Tetrafluoroborate $[BF_4]^-$

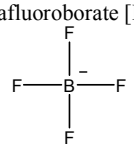

Diethylphosphate $[Et_2PO4]^-$

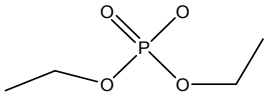

bis[(trifluoromethyl)sulfonyl]imide$[NTf_2]^-$

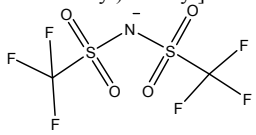

Hexafluorophosphate $[PF_6]^-$

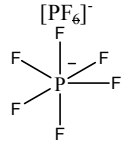

Dimethylphosphate $[Me_2PO4]^-$

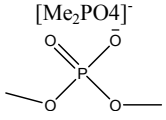

Triflate $[SO_3CF_3]^-$

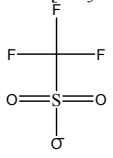

Dicyanamide

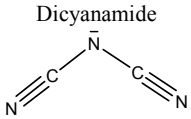

Acetate $[Ac]^-$

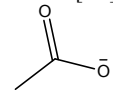

Dihydrogenphosphate $[H_2PO4]^-$

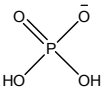

Thiocianate $[SCN]^-$

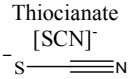

Chloride $[Cl]^-$

Bromide $[Br]^-$

Iodide $[I]^-$

Nitrate $[NO_3]^-$

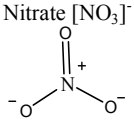

Hidrogensulfate $[HSO4]^-$

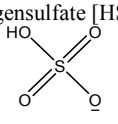

Ethylsulfate $[EtSO4]^-$

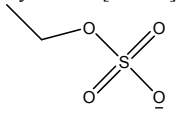

Figure 1

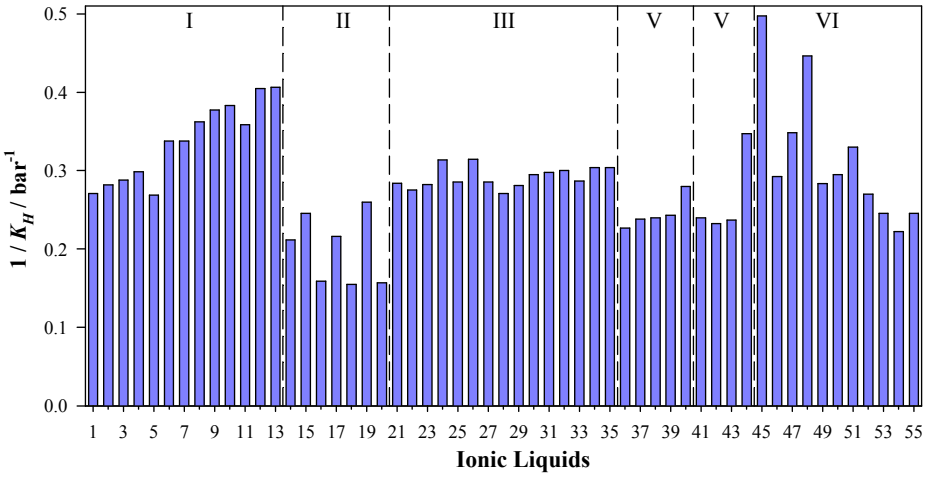

Figure 2

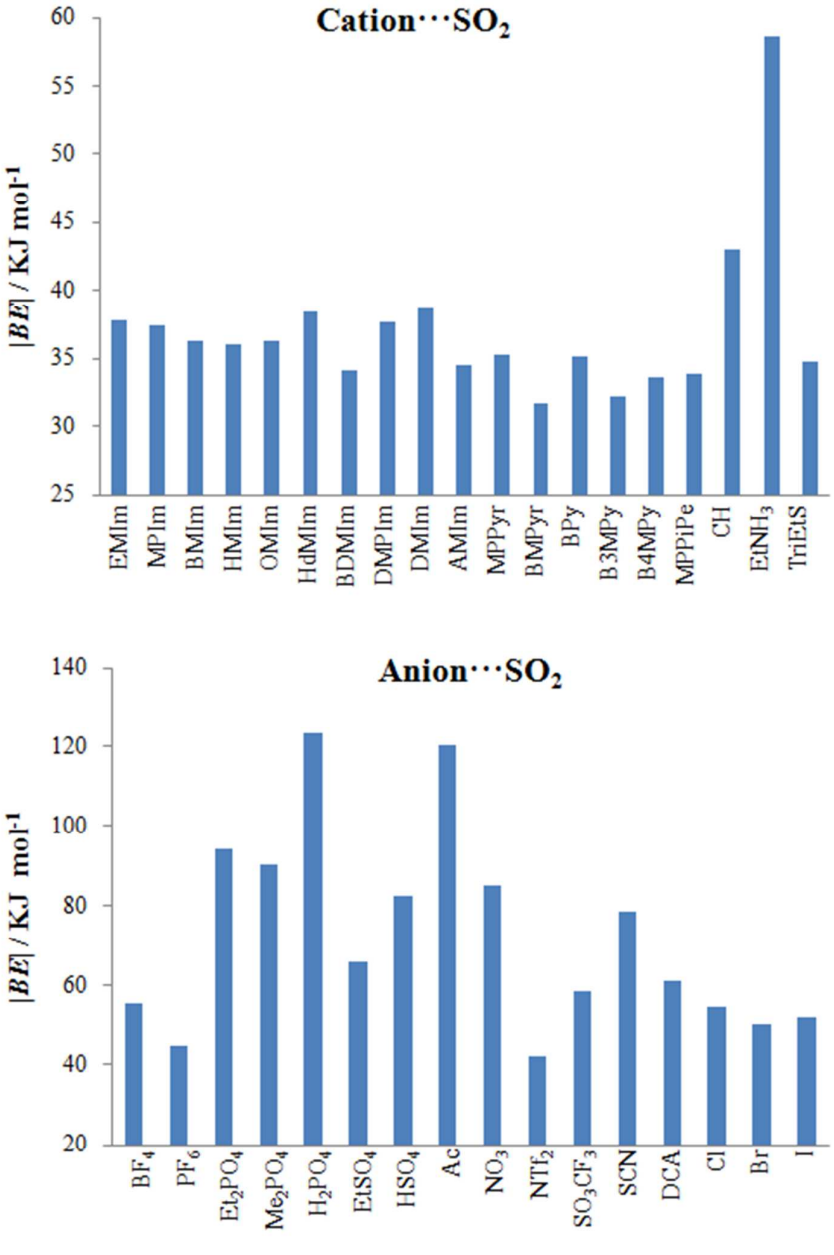

Figure 3

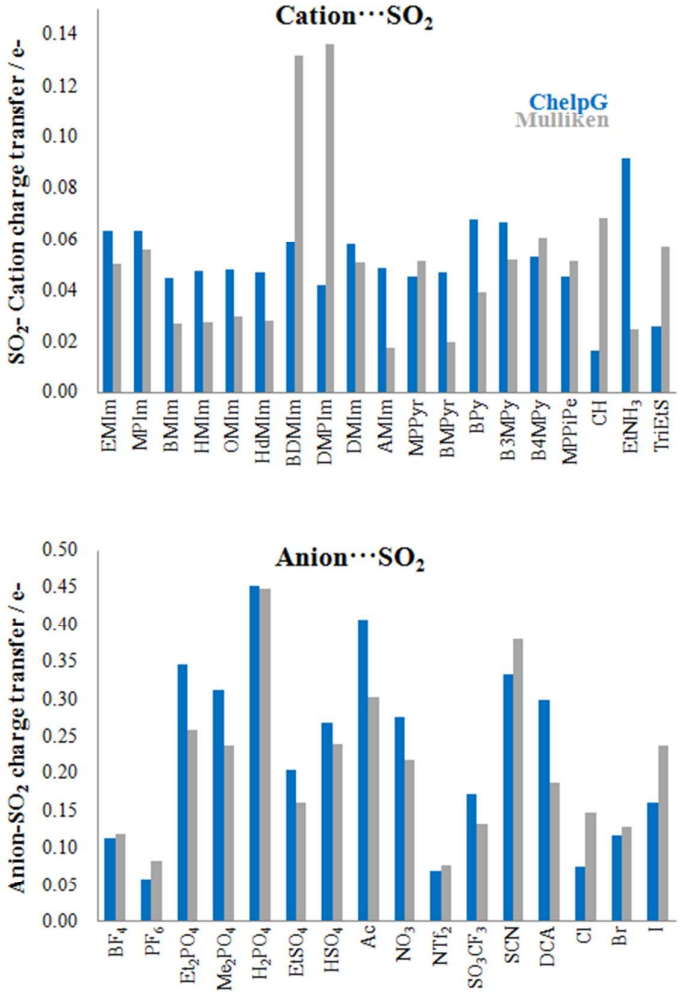

Figure 4

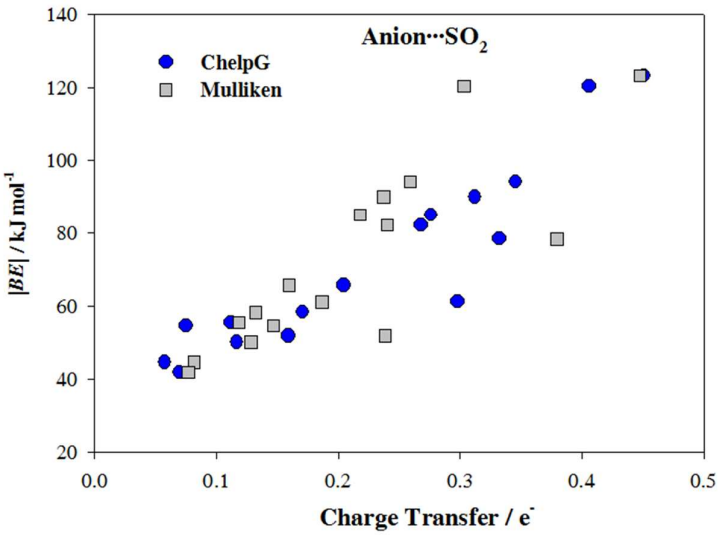

Figure 5

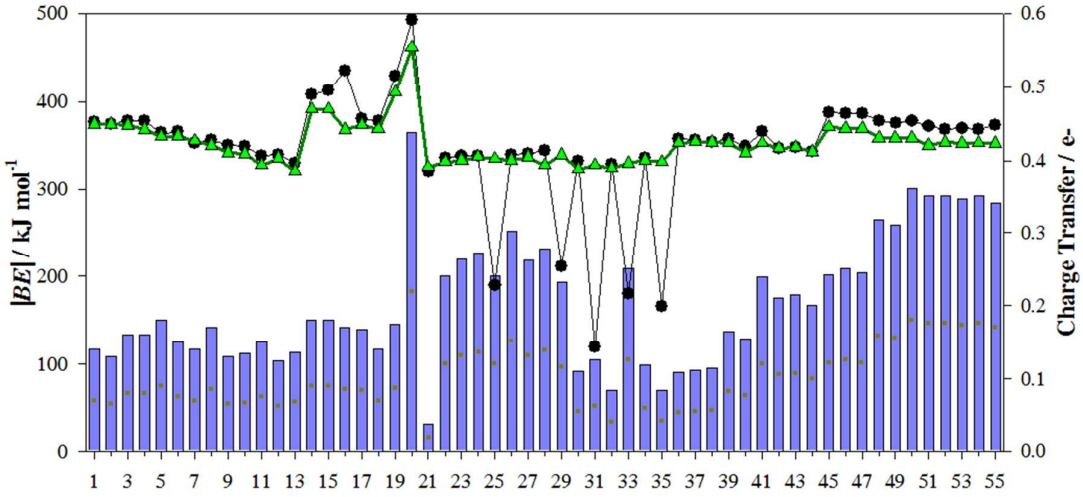

Figure 6

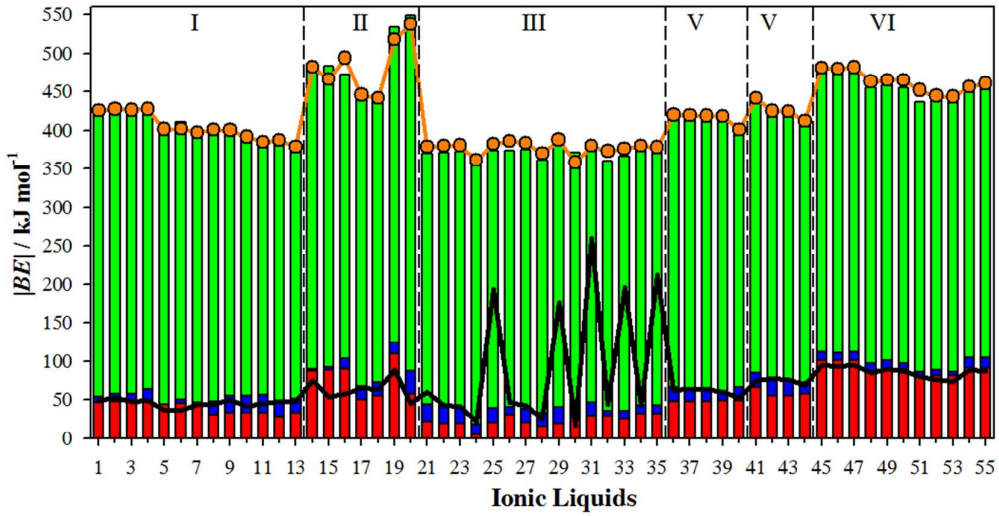

Figure 7

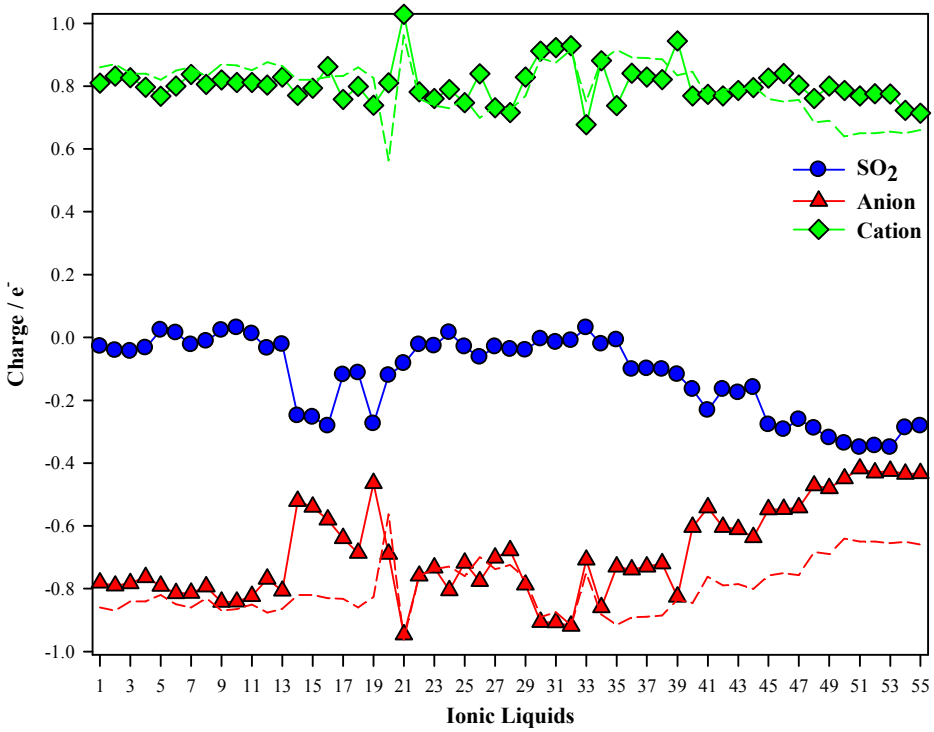

Figure 8

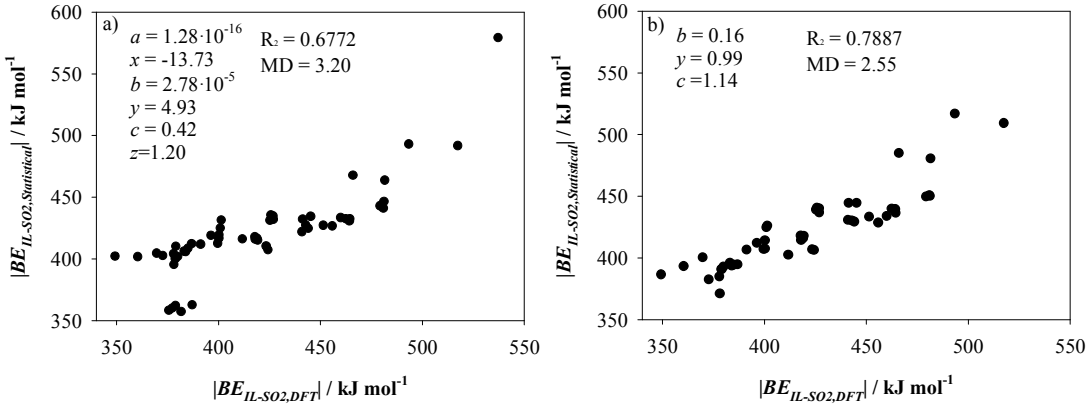

Figure 9

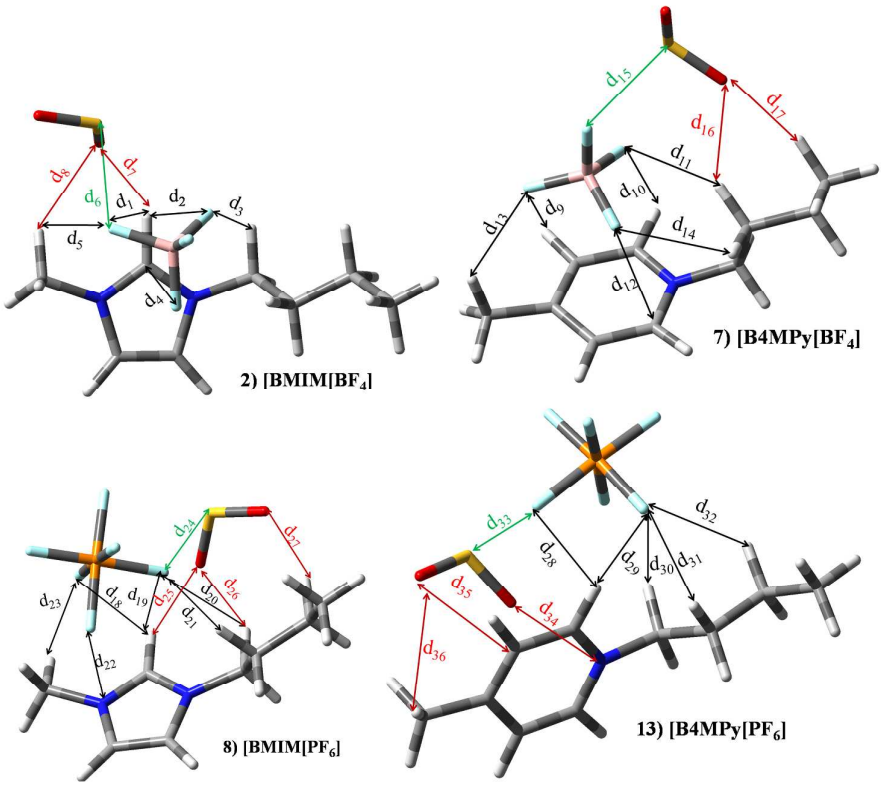

Figure 10

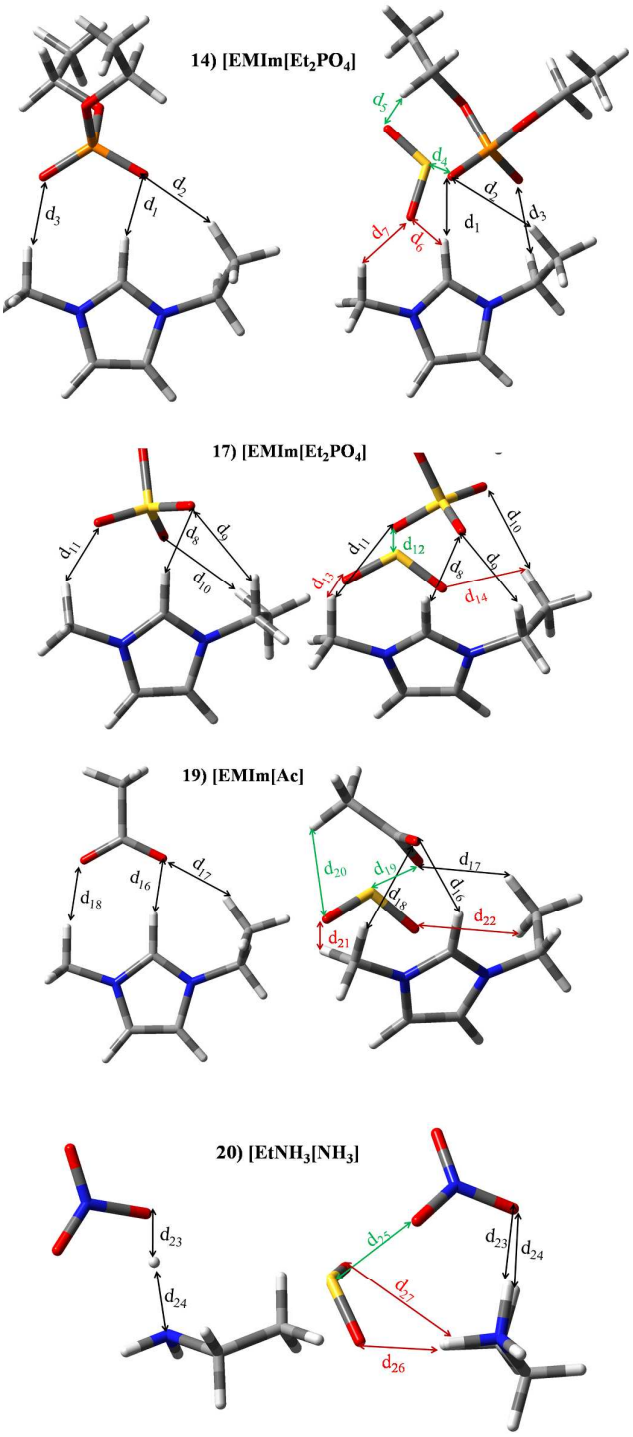

Figure 11

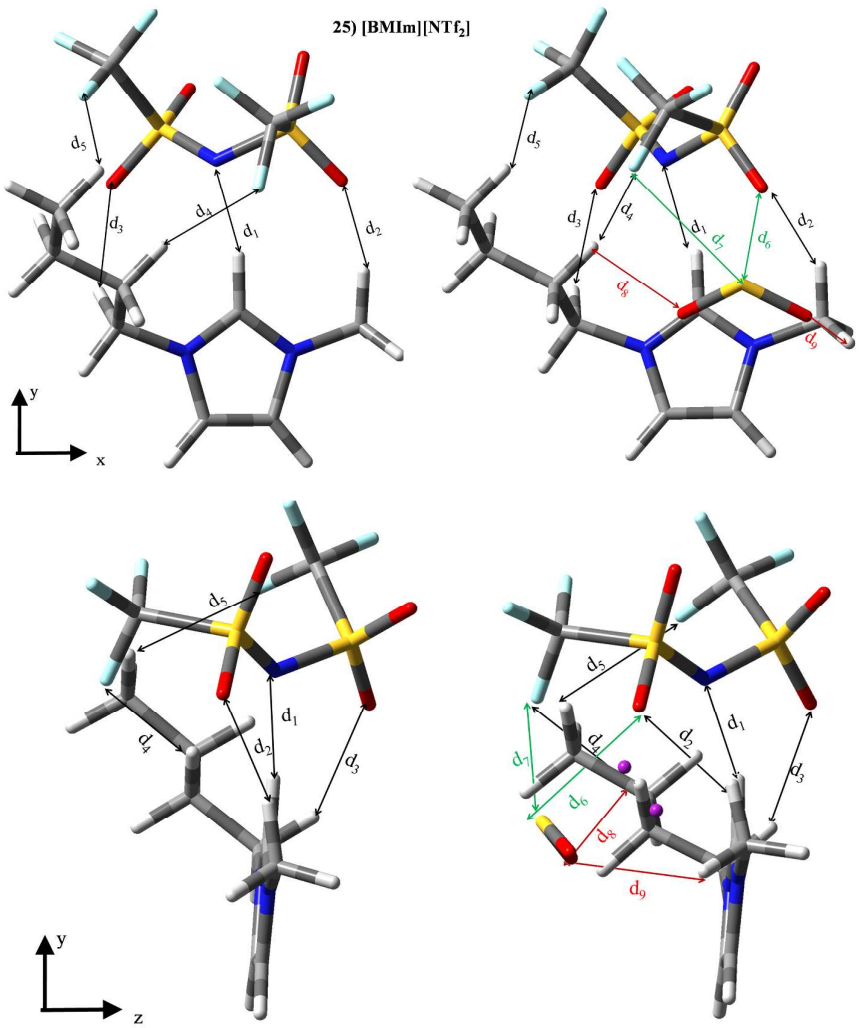

Figure 12

37) [BMIm][SO_3CF_3]

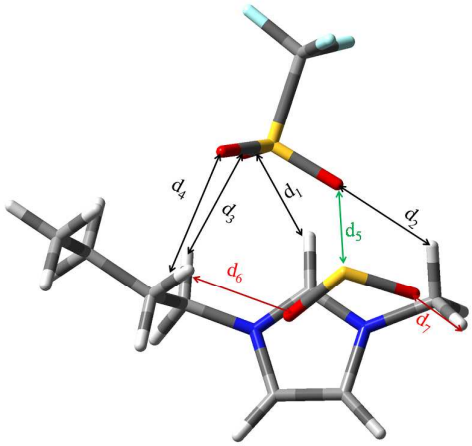

Figure 13

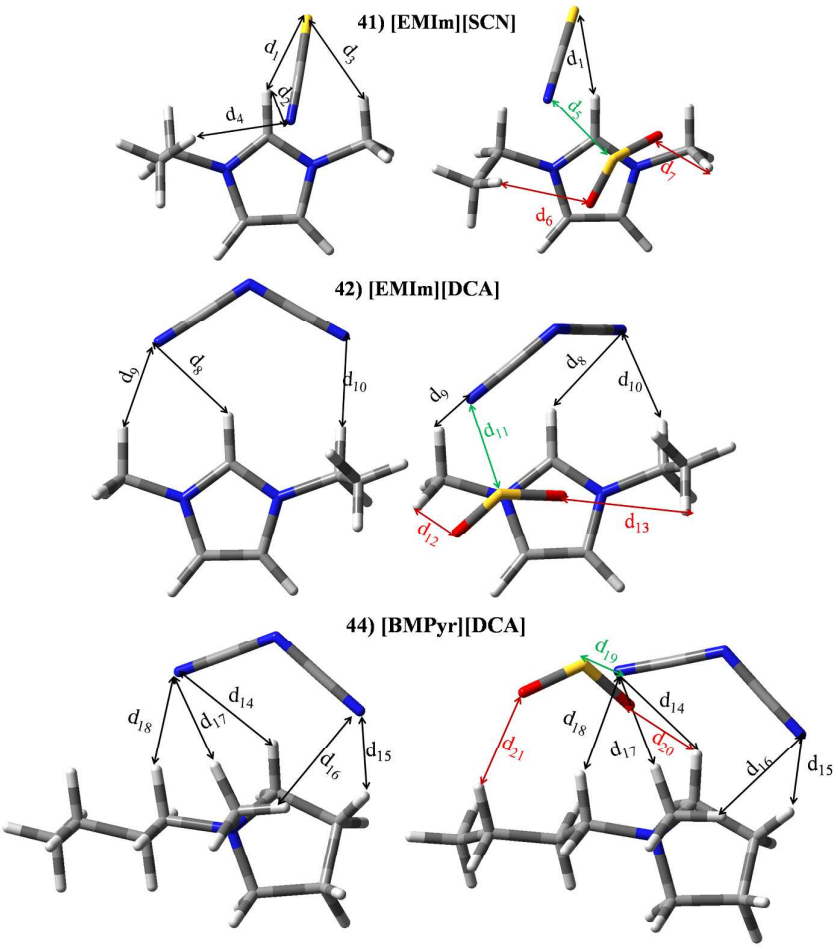

Figure 14

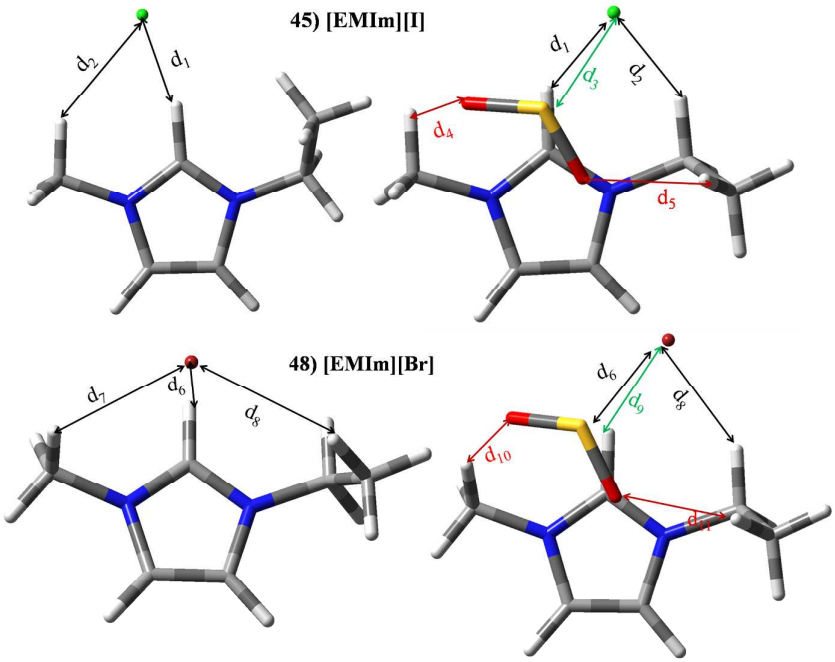

Figure 15